AFRL-RX-WP-TP-2009-4116

PLASTIC FLOW AND MICROSTRUCTURE EVOLUTION DURING LOW TEMPERATURE SUPERPLASTICITY OF ULTRAAFINE Ti-6Al-4V SHEET MATERIAL (PREPRINT)

S.L. Semiatin, P.N. Fagin, J.F. Betten, A. Zane, A.K. Ghosh, and G.A Sargent

Metals Branch
Metals, Ceramics and NDE Division

APRIL 2009

AIR FORCE RESEARCH LABORATORY
MATERIALS AND MANUFACTURING DIRECTORATE
WRIGHT-PATTERSON AIR FORCE BASE, OH 45433-7750
AIR FORCE MATERIEL COMMAND
UNITED STATES AIR FORCE

REPORT DOCUMENTATION PAGE

Form Approved
OMB No. 0704-0188

1. REPORT DATE *(DD-MM-YY)*	2. REPORT TYPE	3. DATES COVERED *(From - To)*
April 2009	Journal Article Preprint	01 April 2009- 01 April 2009

4. TITLE AND SUBTITLE
PLASTIC FLOW AND MICROSTRUCTURE EVOLUTION DURING LOW TEMPERATURE SUPERPLASTICITY OF ULTRAFINE Ti-6Al-4V SHEET MATERIAL (PREPRINT)

5a. CONTRACT NUMBER
In-house

5b. GRANT NUMBER

5c. PROGRAM ELEMENT NUMBER
62102F

6. AUTHOR(S)
S.L. Semiatin (AFRL/RXLMP)
P.N. Fagin and G.A. Sargent (UES, Inc.)
J.F. Betten (Central State University)
A.K. Ghosh (University of Michigan)

5d. PROJECT NUMBER
4347

5e. TASK NUMBER
RG

5f. WORK UNIT NUMBER
M02R2000

7. PERFORMING ORGANIZATION NAME(S) AND ADDRESS(ES)

Metals Branch (RXLMP)
Metals, Ceramics and NDE Division
Materials and Manufacturing Directorate
Wright-Patterson Air Force Base, OH 45433-7750
Air Force Materiel Command, United States Air Force

UES, Inc., Dayton, OH
Central State U, Wilberforce, OH
University of Michigan, Ann Arbor, MI

8. PERFORMING ORGANIZATION REPORT NUMBER
AFRL-RX-WP-TP-2009-4116

9. SPONSORING/MONITORING AGENCY NAME(S) AND ADDRESS(ES)
Air Force Research Laboratory
Materials and Manufacturing Directorate
Wright-Patterson Air Force Base, OH 45433-7750
Air Force Materiel Command
United States Air Force

10. SPONSORING/MONITORING AGENCY ACRONYM(S)
AFRL/RXLMP

11. SPONSORING/MONITORING AGENCY REPORT NUMBER(S)
AFRL-RX-WP-TP-2009-4116

12. DISTRIBUTION/AVAILABILITY STATEMENT
Approved for public release; distribution unlimited.

13. SUPPLEMENTARY NOTES
To be submitted to Metallurgical & Materials Transactions A
PAO Case Number and clearance date: 88ABW-2009-1484, 10 April 2009.
The U.S. Government is joint author of this work and has the right to use, modify, reproduce, release, perform, display, or disclose the work.

14. ABSTRACT
The low-temperature superplastic flow behavior of two lots of Ti-6Al-4V sheet, each with an ultrafine microstructure, was established by performing tension tests at temperatures of 775 and 815C and true strain rates of 10-4 and 10-3 s-1. The as-received microstructures of the two materials comprised either equiaxed or slightly-elongated alpha particles in a beta matrix. The material with equiaxed-alpha particles exhibited flow hardening which was correlated with concurrent (dynamic) coarsening. The rate of dynamic coarsening was rationalized in terms of static coarsening measurements and the enhancement of kinetics due to pipe diffusion. By contrast, the material with initially elongated alpha particles exhibited comparable flow hardening at the lower strain rate but a complex, near-steady state behavior at the higher strain rate. These latter observations were explained on the basis of evolution of alpha-particle shape and size during straining; dynamic coarsening or dynamic spheroidization was concluded to be most important at the lower and higher strain rates, respectively. The plastic-flow behavior was interpreted in the context of a long-wavelength flow-localization analysis.

15. SUBJECT TERMS
titanium alloys, coarsening, superplasticity, tensile ductility

16. SECURITY CLASSIFICATION OF:			17. LIMITATION OF ABSTRACT:	18. NUMBER OF PAGES	19a. NAME OF RESPONSIBLE PERSON (Monitor)
a. REPORT	b. ABSTRACT	c. THIS PAGE			Sheldon L. Semiatin
Unclassified	Unclassified	Unclassified	SAR	52	19b. TELEPHONE NUMBER *(Include Area Code)* N/A

PLASTIC FLOW AND MICROSTRUCTURE EVOLUTION DURING LOW TEMPERATURE SUPERPLASTICITY OF ULTRAFINE Ti-6Al-4V SHEET MATERIAL

S.L. Semiatin, P.N. Fagin*, J.F. Betten**, A. Zane***, A.K. Ghosh‡, and G.A. Sargent*

Air Force Research Laboratory, Materials and Manufacturing Directorate,
AFRL/RXLM, Wright-Patterson Air Force Base, OH 45433
* UES, Inc., 4401 Dayton-Xenia Road, Dayton, OH 45432
**Manufacturing Engineering Dept, Central State University, Wilberforce, OH 45384
***Chemistry Dept, Wright-State University, Dayton, OH 45435
‡ Materials Science and Engineering Dept, Univ of Michigan, Ann Arbor, MI 48109-2136

ABSTRACT

The low-temperature superplastic flow behavior of two lots of Ti-6Al-4V sheet, each with an ultrafine microstructure, was established by performing tension tests at temperatures of 775 and 815°C and true strain rates of 10^{-4} and 10^{-3} s^{-1}. The as-received microstructures of the two materials comprised either equiaxed or slightly-elongated alpha particles in a beta matrix. The material with equiaxed-alpha particles exhibited flow hardening which was correlated with concurrent (dynamic) coarsening. The rate of dynamic coarsening was rationalized in terms of *static* coarsening measurements and the enhancement of kinetics due to pipe diffusion. By contrast, the material with initially elongated alpha particles exhibited comparable flow hardening at the lower strain rate but a complex, near-steady state behavior at the higher strain rate. These latter observations were explained on the basis of evolution of alpha-particle shape and size during straining; dynamic coarsening or dynamic spheroidization was concluded to be most important at the lower and higher strain rates, respectively. The plastic-flow behavior was interpreted in the context of a long-wavelength flow-localization analysis.

Keywords: titanium alloys, coarsening, superplasticity, tensile ductility

I. INTRODUCTION

The fabrication and mechanical properties of metallic materials with an ultrafine microstructure have received much attention during the last decade [1-3]. Most of this work has focused on single-phase alloys with or without a dispersion of second-phase particles. For example, extensive research has been conducted into the mechanisms of continuous dynamic recrystallization to refine grain size during severe-plastic-deformation (SPD) processes of various sorts, subsequent microstructure stability at intermediate and elevated temperatures, low-temperature/high-strain-rate superplastic (SP) behavior, and post-formed mechanical properties such as strength and ductility. Similar work for two-phase alloys (with a high fraction of second phase) has been much more limited. This is primarily because of the generally poorer workability of these alloys at the low temperatures required to impart an ultrafine microstructure via SPD processing and the special tooling required for both SPD and the mechanical tests required to establish SP characteristics.

Because of their widespread application in the aerospace industry, alpha/beta titanium alloys such as Ti-6Al-4V have been the subject of a number of investigations of SP characteristics and, more recently, methods to develop an ultrafine microstructure. In the wrought condition, these materials comprise hcp alpha-phase particles in a matrix of bcc beta phase. In addition to the alpha-beta interfaces, individual alpha particles and the beta matrix may also contain alpha-alpha boundaries and beta-beta boundaries, respectively. Work from the late 1970s and early 1980s [4, 5] revealed that the optimal SP properties of Ti alloys with alpha particle sizes of the order of 5-10 μm were obtained at temperatures at which the volume fractions of the alpha and beta phases were

approximately equal (e.g., 900°C for Ti-6Al-4V), thus suggesting the importance of sliding at alpha/beta interfaces. In addition, this early work revealed that microstructural instability during SP forming (commonly referred to as grain growth) can give rise to flow hardening, i.e., increasing flow stress with strain [4].

Beginning in the mid 1990s, methods were developed to produce an ultrafine microstructure in alpha/beta titanium alloys such as Ti-6Al-4V. A number of these techniques comprised annealing above the beta transus temperature (at which alpha + beta $\rightarrow$ beta) and water quenching to produce a fine, martensitic-alpha preform microstructure followed by SPD at warm-working temperatures. Severe plastic deformation was imparted by techniques such as sheet rolling [6], multi-directional ('abc') forging [7, 8], equal-channel angular extrusion [9], severe compression under superimposed hydrostatic pressure [10], or high-pressure torsion [11]. By these means, ultrafine Ti-6Al-4V having a microstructural scale of the order of 0.5-2 μm was developed. Unfortunately, the sizes of the alpha particles per se and the alpha grains within each alpha particle were often not clearly differentiated in the reporting of the results from these investigations. Hence, it was difficult to interpret the quantitative relation between microstructure and the SP properties of these materials. Considering the wide range of values of the strain rate sensitivity (0.35 – 0.65) and ductility (400 – 1100 pct.) found at temperatures of 700-800°C, it is likely that the ultrafine microstructures were most likely not identical in the various lots of ultrafine Ti-6Al-4V. Such a conclusion is also suggested by observed variations in plastic flow behavior. At times, true stress-true strain curves have exhibited flow hardening [12, 13], flow softening [14], or a combination of steady-state flow, flow hardening, and flow softening

[9, 15] during tension testing at temperatures of the order of 650-800°C and a strain rate of ~10^{-3} s^{-1}.

Recent research has sought to define more clearly the effect of initial microstructure and microstructural instability on flow response during low-temperature superplastic deformation of Ti-6Al-4V. For instance, Sargent, *et al.* [16] demonstrated a quantitative link between flow hardening and dynamic coarsening of equiaxed alpha particles during the low-temperature superplastic deformation of an ultrafine Ti-6Al-4V billet material tested in compression. The objective of the present work was to further clarify the connection between microstructure and low-temperature superplastic behavior of ultrafine alpha/beta titanium alloys, especially those whose manufacture is done by warm SPD processing. To this end, two lots of ultrafine Ti-6Al-4V sheet with noticeably different initial alpha particle morphologies were tested in tension at 775 and 815°C. The flow behavior was interpreted in terms of the evolution of the shape and size of the alpha particles and the kinetics of dynamic coarsening.

II. MATERIALS AND PROCEDURES

A. *Materials*

The present program utilized two lots of Ti-6Al-4V (denoted Sheet A and Sheet B), which had been manufactured by VSMPO (Verkhnaya Salda, Russia) and supplied to the Air Force Research Laboratory by the Boeing Company (Seattle, WA). The thickness of the sheets was 1.98 mm (Sheet A) or 2.54 (Sheet B). The compositions of the two materials (Table I) were nearly identical. Each material also contained a relatively small amount (~0.1 wt pct.) of chromium and nickel, each of which is within the

normal specification for residual elements in Ti-6Al-4V. Based on the research of Wert and Paton [17], such alloying is typical of commercial Ti-6Al-4V and would be expected to have had minimal effect on superplastic properties.

In contrast to their similar composition, the two lots of Ti-6Al-4V had different microstructures. In both the as-received condition and that following a heat treatment at 775°C for 15 min + water quenching (to better delineate the microstructure), Sheet A comprised relatively equiaxed alpha particles in a matrix of beta phase (Figure 1). (In these and subsequent backscattered-electron images (BSEI) taken in a scanning electron microscope (SEM), the dark phase is alpha and the lighter phase is beta.) The alpha particle size was ~1.88 μm in Sheet A. On the other hand, Sheet B consisted of elongated alpha particles with an average thickness of ~3 μm and an aspect ratio of ~2:1 and, to a lesser degree, some equiaxed-alpha particles (Figure 2). The presence of remnant 'dog-leg' shaped particles in Sheet A and the elongated, unspheroidized alpha particles in Sheet B suggested that the process used by VSMPO to make the sheet materials was similar to that originally developed by Inagaki [6]; i.e., warm rolling of beta-annealed-and-water-quenched plate to breakdown a fine martensitic/lamellar alpha microstructure. Because of the proprietary nature of the process used by VSMPO, however, the source of the difference in microstructure in the two different lots can not be definitively ascertained. Nevertheless, it was found that the 'dog-leg' shaped particles had internal alpha-alpha boundaries of very low misorientation as evidenced by their stability during long-term thermal exposure and deformation.

In the as-received condition, both lots of sheet material exhibited strong crystallographic textures. The (0002) pole figure for Sheet A revealed a texture similar

to the so-called basal-transverse type with a maximum intensity of basal poles of ~17 times random located close to the transverse direction of the sheet (Figure 3a). By contrast, the texture of Sheet B was similar to a basal-normal type with a maximum intensity of 11 times random (Figure 3b).

B. *Experimental Procedures*

1. Tension Tests

Isothermal, constant-strain-rate tension tests were performed to determine the plastic flow behavior and accompanying microstructure evolution for the two program materials. For this purpose, dog-bone specimens with a reduced section 12.7 mm long and 3.18 mm wide (Figure 4) were electric-discharge machined from each sheet. The samples contained shoulders consisting of “flags” and tapered grips ends, whose design was chosen to reduce the amount of deformation outside the reduced section [18].

Tension tests were conducted at 775 and 815°C in a computer-controlled Instron mechanical-testing machine outfitted with a Brew vacuum furnace and programmed to provide a constant true axial strain rate of 10^{-3} or 10^{-4} s^{-1}, assuming uniform deformation within the reduced section. Prior to each test, the furnace was evacuated to 10^{-6} torr. The test sample was then heated to test temperature in 20 minutes under load control (to prevent buckling) and soaked at temperature for 15 minutes before testing under stroke control. Most tests were taken to a true axial strain of ~1.9. Because of the 89-mm maximum crosshead travel of the system (corresponding to an average axial strain of ~2.1), only a few tests could be taken to failure with the current sample design.

Flow curves were determined from the load-stroke data using standard formulas and the assumption of uniform deformation (prior to the onset of localized necking) that had been confined to the reduced section. Post-test measurements revealed a small amount of deformation outside the gage section (~0.05 strain at an overall strain of 1.8). However, such errors did not affect the overall shape of the flow curves or the interpretation of the present results.

Selected strain-rate jump tests were also conducted at 775 and 815°C to determine the strain-rate sensitivity of the flow stress (m value) and thus aid in the analysis of the flow response. These tests comprised strain-rate changes between 10^{-3} and $3x10^{-3}$ s^{-1} or between $3x10^{-3}$ and 10^{-2} s^{-1} at true strain intervals of 0.05. The m values were calculated from the loads P_1 and P_2 just before and after the jump and the two strain rates $\dot{\varepsilon}_1$ and $\dot{\varepsilon}_2$, i.e., $m = [\log(P_2/P_1)] / [\log(\dot{\varepsilon}_2/\dot{\varepsilon}_1)]$.

2. Metallography

Extensive metallography was conducted following tension testing to quantify dynamic coarsening behavior and the aspect ratio of each phase. Because water quenching was not possible in the evacuated mechanical-testing system, each tension sample was encapsulated in a quartz tube following deformation, reheated quickly to its test temperature, held for 15 minutes to equilibrate the microstructure without inducing measurable additional coarsening, and then water quenched. Subsequently, samples were sectioned axially and prepared using standard metallographic techniques. A series of 2 to 4 BSEI photographs was taken at various locations along the gage section in the mid-thickness region. Magnifications were chosen to ensure that ~100-800 total particles were sampled in the collection of micrographs for each test condition. The

average alpha particle size, A_α, was determined by counting the number of particles, N_α, measuring the volume fraction of alpha, f_α, in each micrograph, and applying the relation $A_\alpha = f_\alpha A_T/N_\alpha$, in which A_T denotes the area of the micrograph. Those particles consisting of a 'dog-leg' geometry were counted as being 1.5 particles in number to provide an approximate estimate of the effect of their radii of curvature on coarsening behavior. The average alpha particle radius, $\bar{r}_\alpha$, was estimated from the value of A_α based on a circle with equivalent area. The average alpha-particle radius ($\bar{r}_\alpha$) and beta-grain radius ($\bar{r}_\beta$) were also determined using a linear-intercept technique. The two techniques showed excellent agreement. The overall uncertainty of the average particle/grain size measurements was estimated to be approximately ± 5 pct.

Additional, individual measurements of the geometry of alpha particles and beta grains were used to determine the aspect ratio of the phases before and after deformation.

Observations of the coarsening of alpha particles during tension testing of Sheet A samples were compared to measurements of *static* coarsening of samples of this material which had been statically heat treated at 775 and 815°C for times ranging from 15 min to 96 hours.

C. *Flow-Localization Analysis*

A flow-localization analysis was conducted to assess the influence of strain-rate sensitivity and flow hardening on stress-strain response and the development of strain non-uniformity during low-temperature superplastic deformation of Ti-6Al-4V sheet with

an ultrafine microstructure. For this purpose, a simple load-equilibrium approach identical to that used in the past [19, 20] was employed.

The analysis was implemented using a spreadsheet calculation in which symmetry about the mid-length was assumed. Hence, attention was focused on one-half of the tension specimen which was divided into six slices of initially equal length. (Simulations with a greater number of slices gave essentially identical results.) A linear variation of gage width/area from the (non-deforming) shoulder to the center of the specimen was assumed. The samples used in the experiments had a 1 pct. taper. Hence, the numerical simulations assumed an overall initial geometric defect size ($1 - f_o$) of 0.01 or 0.02. The latter value was chosen in order to incorporate the influence of both intrinsic geometry variations and initial strength variations. The spreadsheet calculations comprised relating the strain rate in each slice to that of the outermost slice, subject to the boundary condition of a constant overall true strain rate within the gage section. The development of stress triaxiality due to the development of a diffuse neck was neglected. Model outputs included predictions of the apparent true stress - true strain response during diffuse necking and the strain profile in deformed tension specimens.

III. RESULTS AND DISCUSSION

The principal results from this investigation related to the plastic flow behavior and microstructure evolution of the two lots of Ti-6Al-4V sheet material and the interpretation of these observations in terms of a simple flow-localization analysis. The findings in each area are summarized and discussed in the following sections.

A. *Plastic-Flow Behavior*

1. Flow Curves

The flow response of the two lots of Ti-6Al-4V (Figure 5) showed some differences and some similarities to each other and to previous findings for an ultrafine Ti-6Al-4V billet material tested to a true axial strain of ~1 in compression [16]. For example, following yielding, Sheet A revealed flow hardening to large strains (Figure 5a); such behavior was similar to that found for the billet material. The initial yield strengths of Sheet A for deformation at 10^{-4} or 10^{-3} s^{-1} and test temperatures of 775 and 815°C, however, were *higher* than those found for the billet material tested under identical conditions. In addition, the rates of flow hardening were approximately one-half those observed for the billet material. In part, these findings can be ascribed to (1) the coarser starting microstructure (~2.4-μm alpha-particle diameter in Sheet A [taking into account the static coarsening during the longer preheat in tension testing] versus ~1.26-μm alpha-particle diameter in the billet) and (2) the concomitant smaller amount of alpha-particle coarsening during deformation, as will be described in Section III.B.I. The small degree of steady-state flow and flow softening at large strains for Sheet A may be ascribed to the onset/development of diffuse necking and the uniform-flow approximation utilized in reducing load-elongation data to true stress-true strain. This behavior will be discussed further in Section III.C.

The flow curves for Sheet B (Figure 5b) indicated a marked dependence on strain rate. For deformation at 10^{-3} s^{-1}, the true stress-strain curves exhibited a peak stress at low strains (~0.1) followed by noticeable or modest flow softening to a strain of ~1 at temperatures of 775 and 815°C, respectively. At 815°C and 10^{-3} s^{-1}, a small

amount of flow hardening was observed at a strain greater than ~1. By contrast, deformation at 10^{-4} s^{-1} was characterized by marked flow hardening after initial yielding, a behavior very similar to the observations for Sheet A (Figure 5a) and the previous findings for the ultrafine Ti-6Al-4V billet [16]. However, as for Sheet A, the initial yield strengths of Sheet B tested at 10^{-4} s^{-1} were substantially higher (by approximately a factor of two) than those found for the billet material tested at the same temperatures, and the rate of flow hardening was approximately one-half that of the billet material. Again, such findings can be ascribed to the coarser initial microstructure and reduced level of dynamic coarsening for Sheet B. Dynamic spheroidization of the microstructure must be considered to explain the observed strain rate dependence of plastic flow for Sheet B, however.

2. Strain-Rate Sensitivity of the Flow Stress

Measurements of the strain-rate sensitivity of the flow stress (m values) provided insight into the mechanism of plastic flow. The m values showed a noticeable dependence on strain rate and strain, but were similar for the two sheet materials (Figure 6).

For the strain-rate range between 10^{-3} and $3x10^{-3}$ s^{-1}, m values were ~0.65 at 775°C or ~0.75 at 815°C and decreased slightly with deformation starting at strains of ~1. These m's are comparable to those found previously for the ultrafine Ti-6Al-4V billet material tested in compression [16] and are of a magnitude considered to be requisite for superplastic flow characterized by grain/phase-boundary sliding (gbs). Furthermore, the corresponding values of the stress exponent n (= 1/m) were ~1.33 - 1.5. This suggests that gbs was likely accommodated to various degrees by dislocation glide-

climb (which would yield n = 2, as in the core-mantle model of Gifkins [21]) and diffusional processes (for which n = 1). Pole figures measured following deformation (e.g., Figure 7) showed a marked reduction of the texture intensity for both Sheet A and Sheet B, thus underscoring the likelihood of boundary sliding as suggested by the m-value measurements. Moreover, measurements of the normal plastic anisotropy (i.e., r~ width strain/thickness strain) at the end of the large-strain deformation of Sheet A were approximately equal to unity. Such r values suggest as well that crystallographic slip, which would produce very low r's for the sharply textured Sheet A pulled along the RD, played a minor role in the plastic flow process.

For jump tests using strain rates of $3x10^{-3}$ and 10^{-2} s^{-1}, the m values were lower by approximately 0.1 – 0.15 at a strain of 0.1, and thereafter showed a monotonic decrease with further deformation (Figure 6). In fact, the m values had decreased to ~03 for Sheet A and to ~0.2 for Sheet B after reaching a strain of ~1.5; these latter m values are typical of power-law creep (plc) deformation. The decrease in m with strain and the transition to plc-type deformation in this higher strain-rate regime is likely associated with dynamic coarsening (to be discussed below). In addition, these decreases could have an effect on flow stability at large strains for tests conducted at 10^{-3} s^{-1}. In such cases, the strain-localization process could be exacerbated by higher local strain rates and the accompanying lower m values at the center of the diffuse neck [19].

B. *Microstructure Evolution*

The observed plastic flow response was found to be related to dynamic microstructural changes which were different for the two lots of Ti-6Al-4V sheet and thus are discussed separately.

1. Sheet A

Sheet A, which consisted of relatively-equiaxed alpha particles in the as-received condition and which exhibited flow hardening, underwent dynamic coarsening during deformation at both 775 and 815°C (e.g., Figures 8 and 9 for 775°C and the two different strain rates). Micrographs taken at various locations along the deformed gage section revealed that the degree of coarsening was not measurably dependent on local strain; a similar behavior was found in the investigation of dynamic coarsening of Ti-6Al-4V during hot compression testing with its associated friction-induced strain non-uniformity [22]. Based on this finding, an approximate dynamic coarsening rate K_d was fit to the observations at the beginning and end of each tension test. Per previous findings related to the coarsening of ultrafine Ti-6Al-4V billet material tested in compression [16], it was assumed the average particle size $\bar{r}_{\alpha o}$ followed a cubic dependence on time t, viz:

$$\bar{r}_{\alpha}^{3} - \bar{r}_{\alpha o}^{3} = K_d(t - t_o) \, . \qquad (1)$$

In Equation (1), the subscript “o” refers to the pertinent quantities at some prescribed initial time t_o. Specifically, $\bar{r}_{\alpha o}$ was taken to be the average alpha-particle radius at the end of the heating-plus-soak time in the tension tests. The coarsening rates based on the average particle radius at this time and the time at the conclusion of the tension test are summarized in Table II.

To assess the possible enhancement of coarsening kinetics due to concurrent deformation, the measured dynamic coarsening rates were compared to *static*-coarsening data for Sheet A. Noticeable static coarsening was noted at both 775°C

(Figure 10) and 815°C (not shown). Much like the behavior of the ultrafine Ti-6Al-4V billet material [16], the static coarsening of Sheet A revealed a cubic dependence of the alpha-particle radius on time for both heat-treatment temperatures (Figure 11a), thus suggesting that coarsening was controlled by solute diffusion through the beta matrix. The static coarsening rates (K_s) fit to these data were 0.56 $\mu m^3/h$ at 775°C and 0.87 $\mu m^3/h$ at 815°C. These values are very similar to those found for the low-temperature static coarsening of the ultrafine Ti-6Al-4V billet, i.e., 0.66 $\mu m^3/h$ at 775°C and 0.83 $\mu m^3/h$ at 815°C as well as corresponding predictions from a modified Lifshitz-Slyosov-Wagner (LSW) analysis discussed in Reference 16. Similar to the previous observations for the billet material, the static coarsening of the *beta* grains in Sheet A was also found to be related to that of the alpha particles through a Zener-like relation of the following form:

$$\bar{r}_\alpha = C\bar{r}_\beta / f_\beta \quad . \qquad (2)$$

Here, $\bar{r}_\beta$ denotes the average beta grain size, and C is a constant. For classic Zener grain-boundary-pinning behavior (typically found for small volume fractions of second-phase beta pinning grains denoted as alpha), the value of C is 2/3. In the present work, a linear relation between $\bar{r}_\alpha$ and $\bar{r}_\beta / f_\beta$ was found (Figure 11b) with slope C equal to 0.41 at 775°C and 0.57 at 815°C. These values of C bracket that found for the ultrafine Ti-6Al-4V billet, i.e., 0.43.

A comparison of the static and dynamic coarsening rates for Sheet A (Table II) revealed that K_d was approximately 7-20 times as large as K_s. This enhancement of coarsening kinetics due to concurrent deformation was similar to that found previously

during superplastic defomation in compression of ultrafine Ti-6Al-4V billet material at low-temperatures (~10-fold increase) [16] and high-temperatures (~5-fold increase) [22]. As noted previously, this increase can be attributed to pipe diffusion associated with the generation of dislocation substructure in the beta phase through which solutes are being transported. Such an explanation can also be used to rationalize the absence of a strong dependence of dynamic-coarsening behavior on strain during diffuse necking in tension. In particular, because mechanisms of deformation tend to vary as the *logarithm* of the applied strain rate, a several fold variation of strain rate over the length of a deforming tension specimen would not be expected to give rise to major differences in solute diffusivity. To a first order, therefore, the influence of dynamic coarsening on plastic flow for a somewhat narrow range in strain rate can be modeled in terms of its *temporal* effect on the strength coefficient in engineering (phenomenological) flow laws.

The dynamic coarsening in tension was used to obtain a quantitative explanation of the observed levels of flow hardening for Sheet A (Figure 5a). For this purpose, the generalized constitutive relation of Bird, Mukherjee, and Dorn [23] was applied, as in previous work for the compressive flow of ultrafine Ti-6Al-4V billet [16], i.e.,

$$\dot{\varepsilon} = \left(\frac{ADGb}{kT}\right)\left(\frac{\sigma}{G}\right)^{n}\left(\frac{b}{d}\right)^{p} \quad . \qquad (3)$$

In this relation, A is a constant, D is a diffusivity, G is the shear modulus, b is the length of the Burgers vector, k is Boltzmann's constant, T is absolute temperature, σ is the flow stress, d is the average alpha-particle *diameter*, n is the stress exponent of the strain rate (=1/m), and p is the grain size exponent of the strain rate. At fixed temperature and strain rate, the flow stress should thus vary with d according to the following equation:

$$\sigma \sim d^{p/n} \quad . \qquad (4)$$

For the Sheet A tension tests at 10^{-3} s^{-1}, n = 1.33 (=1/0.75, per Figure 6a). Per previous work [16], the value of p is ~2. Thus, the flow stress should vary as the alpha particle diameter to the power of 1.5 (=2/1.33). For the 10^{-3} s^{-1} flow curves shown in Figure 5a, the alpha-particle diameter grew from 2.40 to 3.76 μm (775°C) or from 2.45 to 4.40 μm (815°C). Thus, the predicted increase of flow stress due to dynamic coarsening would be approximately $(3.76/2.4)^{1.5}$, or 1.97 times the initial flow stress, at 775°C or $(4.40/2.45)^{1.5}$, or 2.41 times the initial flow stress, at 815°C. These values are in semi-quantitative agreement with the flow stress measurements in Figure 5a, which show an increase of 1.76 times the initial flow stress at 775°C and 2.13 times the initial flow stress at 815°C. *

2. Sheet B

As for Sheet A, the microstructure along the length of Sheet B samples following tension testing was affected to only a very minor degree by the variation in local strain due to diffuse necking (e.g., Figures 12, 13). However, the specific mechanism of microstructure evolution was not as straightforward. For example, deformation at 775°C led to coarsening *and* spheroidization (Figures 12, 13). After relatively large strains (~2), there remained only slight evidence of remnant alpha lamella. Because the remnant lamellae in the starting material were relatively thick, however, it is likely that dynamic

* Because of variations in stress and strain rate in the diffuse neck, the flow stress at the end of each tension test was obtained by extrapolating the portion of flow curve *prior to* diffuse necking to the final average true strain.

spheroidization occurred not due to boundary splitting [24, 25] but rather as a result of mass transport from the end to the center of the same or adjacent lamellae [26].

Despite the mixed equiaxed-lamellar starting microstructure, Sheet B exhibited relatively high m values, as discussed in Section III.A.2 (Figure 6b). This may be due to a combination of several factors including (a) the presence of a non-negligible fraction of fine equiaxed-alpha particles prior to the onset of deformation, (b) an increase in the fraction of equiaxed particles due to spheroidization as deformation proceeded [27], and (c) cooperative phase-boundary sliding [28]. The latter mechanism, characterized by the sliding in a cooperative manner of entities comprising groups of particles, may be important in mitigating the influence of remnant lamellae on the overall plastic-flow behavior.

Because of the complexity of the microstructure evolution in Sheet B samples, it is difficult to interpret its precise effect on plastic flow. However, a comparison of the flow curves for sheets A and B may be used to formulate a reasonable hypothesis. For deformation at 10^{-3} s^{-1}, the flow stresses of Sheet B at low strains were approximately 50 pct. higher than those for Sheet A at each of the two test temperatures (Figure 5). Because Sheet B exhibited high m values at this strain rate (Figure 6), its plastic flow was likely characterized by some form of boundary sliding. Using Equation (4) with p/n = 1.5 and the measured higher flow stresses in Sheet B, an “effective” particle diameter can be estimated. Specifically, the ratio of the initial effective particle diameter in Sheet B to the initial particle diameter of Sheet A would be $1.5^{1/1.5} \sim 1.3$. This would imply an effective particle diameter of 1.3 x 2.4 μm, or 3.1 μm, a value which is comparable to the initial platelet thickness of the unspheroidized portion of the microstructure as well

as the diameter of spheroidized particles that form a portion of the starting microstructure of Sheet B. At a strain of 1.5, the flow stresses of Sheet B were comparable to or slightly less than those for Sheet A. Microstructures at this level of strain were very similar in Sheets A and B (Figures 8, 12). Hence, the flow softening noted for Sheet B at 10^{-3} s^{-1} is likely related to a coupled dynamic spheroidization/coarsening process.

Because of the tenfold longer duration, flow behavior during tension testing of Sheet B at a strain rate of 10^{-4} s^{-1} would have been dominated by the relatively large degree of dynamic coarsening (Figure 13) with spheroidization likely occurring during the initial straining and playing much less of a role. Hence, flow curves for this lower strain rate showed essentially continuous flow hardening (Figure 5b).

To confirm and quantify the importance of dynamic spheroidization on the flow behavior of Sheet B, the time required to globularize remnant, pancake-shape alpha lamellae via volume diffusion τ_{vd} was estimated using a model developed by Semiatin, *et al*. [26]. Per this earlier work, the final result for *static* spheroidization is the following:

$$\frac{\tau_{vd}}{\tau'} = \frac{\xi^3 - [0.328\xi^{7/3}\left(1+\sqrt{1-0.763\xi^{-4/3}}\right)^2]}{4[\frac{2(1+\xi)}{3(0.5-0.572\xi^{-1/3})} + \frac{0.5\xi^{1/3}+0.665\xi^{2/3}}{3(0.143+0.934\xi^{-1/3})}]} \qquad (5a)$$

in which

$$\xi \equiv (w/d_\alpha) + 0.5 \qquad (5b)$$

$$\tau' \equiv d_\alpha^3 R_g T/D_\beta C_F \gamma_{\alpha\beta} V_M \qquad (5c)$$

In Equations (5), w and d_α denote the alpha platelet diameter and thickness, respectively, R_g is the gas constant, T is the absolute temperature, D_β is the diffusivity of the rate limiting solute in beta titanium (under static conditions), C_F is a composition correction factor, $\gamma_{\alpha\beta}$ is the alpha/beta interface energy, and V_M is the molar volume.

For the present case, the static diffusivity D_β (in $\mu m^2/s$) is equal to 0.0045 (775°C) or 0.0083 (815°C), C_F is equal to 11.8 (775°C) or 15.6 (815°C) , $\gamma_{\alpha\beta}$ = 0.4 J/m^2, and V_M = 1.044 x 10^{-5} m^3/mol. Using these values as input, the *static* spheroidization time for remnant lamellae which are 3 μm thick and have an aspect ratio of 2:1 was predicted to be 15.3 h (775°C) or 6.3 h (815°C).

Per the results in Table II, concurrent deformation at a strain rate of 10^{-3} s^{-1} increases the kinetics of diffusion-controlled processes by a factor of ~17. Hence, the time required for dynamic spheroidization would be 0.90 h (775°C) or 0.37 h (815°C), corresponding to strains of either ~3.2 (775°C) or ~1.3 (815°C). Referring to the 10^{-3} s^{-1} flow curves for sheet B (Figure 5b), the absence of flow hardening after a strain of ~2 (775°C) and the beginning of flow hardening at a strain of ~1 (815°C) can thus be readily rationalized.

For concurrent deformation at a strain rate of 10^{-4} s^{-1}, kinetics increase by a factor of ~7.5 relative to those for a static process (Table II). The time required for dynamic spheroidization would therefore be 2.04 h (775°C) or 0.84 h (815°C), corresponding to strains of either ~0.7 (775°C) or ~0.3 (815°C), respectively. The observed flow hardening at all strains at 815°C (Figure 5b) seems reasonable therefore.

The presence of only a short initial retardation of flow hardening (for a strain increment of ~0.2) at 775°C suggests that refinements in the analysis would be useful.

C. *Flow-Localization Analysis*

The flow-localization analysis was useful in explaining the shape of the observed flow curves at large strains during which diffuse necking had occurred. Microstructure observations (summarized in Section III.B) enabled a substantial simplification of the flow-localization formulation. In particular, it was observed that microstructure evolution was relatively uniform along the entire gage section despite the development of a diffuse neck. Hence, the observed flow hardening/softening was not *strain* hardening/softening per se, but rather an indication of the temporal evolution of the strength coefficient K. For this reason, the pertinent (phenomenological) constitutive equation was taken to be the following

$$\sigma = K(t)[(\dot{\varepsilon}/\dot{\varepsilon}_o)^m] , \qquad (5)$$

and the corresponding load-equilibrium equation, neglecting the small stress triaxiality in the diffuse neck, was

$$\delta P = \delta\{\sigma_x A\} = \delta\{K(t)[(\dot{\varepsilon}/\dot{\varepsilon}_o)^m] A\} = 0 . \qquad (6)$$

In Equations (5) and (6), δP denotes the variation of the axial load P along the gage length; σ_x, the axial stress, $\dot{\varepsilon}$, the axial strain rate, and A, the cross-sectional area, are functions of the axial coordinate x; and $\dot{\varepsilon}_o$ denotes a (constant) reference strain rate, typically taken to be the average true (or nominal) strain rate imposed during the tension test.

The simulation of flow localization for a non-flow-hardening material (K(t) = constant = 100, in arbitrary units) with m = 0.5 and f_o = 0.98 (Figure 14a) revealed the important features of the stress-strain response. Not unexpectedly, the *engineering* stress-strain curve showed a smooth decrease following load instability at zero strain. From such curves, it was not apparent when diffuse necking began. This behavior contrasted with the true stress - true strain curve calculated from the simulated load and the assumption of uniform deformation along the gage length. In this case, there *was* a noticeable drop in stress (at a strain of ~1.5) at which the neck began to form. It should be noted that this drop in true stress did not underlie a material property per se, for the material was assumed to be perfectly viscoplastic. Rather, it is a result of the beginning of a marked deviation from the assumption of uniform deformation due to diffuse necking during the tension test.

A similar behavior in true stress – true strain curves was found for cases involving flow hardening, as shown in Figure 14b. In this figure, the simulated true stress – true strain curve for the non-hardening case from Figure 14a is compared to that for a simulation with identical values of m and f_o, but for which K increased from 100 to 150 during the time required to impart a strain of 2. This flow hardening led to a broadening of the stress-strain curve at the peak stress but did not markedly affect the strain at which the curve started to decrease noticeably.

Related simulation results for a non-hardening constitutive behavior with m = 0.35, 0.5, or 0.75 and f_o = 0.98 or 0.99 (Figure 15) quantified more fully the effect of material parameters on apparent true stress – true strain curves and the development of strain non-uniformity. In particular, the results in Figure 15b for an overall axial true

strain of 1.9 indicate that measurable strain non-uniformity does indeed correlate to those cases exhibiting noticeably decreasing true stress – true strain curves at this strain.

The results from the flow-localization analysis explained at least qualitatively some of the principal features of the measured flow response. A direct comparison was not possible because m was taken as constant in each simulation, unlike the actual experimental behavior (Figure 6). Nevertheless, the basic shape of the predicted flow curves for an m comparable to that in the experiments (i.e., 0.5) and f_o = 0.98 (Figure 14b) was indeed similar to the experimental results for the cases in which flow hardening did or did not occur (Figure 5). Furthermore, predicted strain profiles were found to be comparable to measurements.

IV. SUMMARY AND CONCLUSIONS

The low-temperature superplastic flow behavior of two lots of Ti-6Al-4V sheet, each with an ultrafine microstructure, was determined using constant strain rate tension tests. The principal conclusions of this work are as follows:

1. Plastic flow of ultrafine Ti-6Al-4V at temperatures of 775 and 815°C is superplastic at strain rates of 10^{-3} and 10^{-4} s^{-1}, with m values of the order of 0.5 – 0.75 and total elongations in excess of 700 pct.

2. Sheet with an ultrafine, fully-wrought microstructure of equiaxed-alpha particles in a beta matrix exhibits flow hardening as a result of dynamic coarsening. The rate of dynamic coarsening is ~10-20 times as rapid as the corresponding static-

coarsening rate as a result of concurrent deformation and enhanced (pipe) diffusion of the solutes which control coarsening.

3. Sheet with a mixed starting microstructure of equiaxed and remnant-lamellar alpha shows a strain-rate-dependent flow behavior. At 10^{-3} s^{-1}, the softening influence of dynamic spheroidization competes with the hardening influence of dynamic coarsening, resulting in near steady-state flow. By contrast, deformation at 10^{-4} s^{-1} gives rise to a flow-hardening behavior because dynamic coarsening dominates microstructure evolution.

4. Despite the occurrence of diffuse necking and the evolution of concomitant strain gradients, the microstructure developed during low-temperature superplastic flow of ultrafine Ti-6Al-4V is relatively uniform. This suggests that constitutive behavior can be described as rate sensitive with a strength coefficient which is a function of time for a given imposed strain rate.

5. Reduction of load-elongation data to true stress – true strain assuming uniform deformation may lead to an apparent, but physically artificial, flow-softening response during nominally quasi-stable diffuse necking.

Acknowledgements – This work was conducted as part of the in-house research of the Metals Processing Group of the Air Force Research Laboratory's Materials and Manufacturing Directorate. The support and encouragement of the Laboratory management and the Air Force Office of Scientific Research (Dr. J. Fuller, program manager) are gratefully acknowledged. One of the authors (GAS) was supported under Air Force contract FA8650-04-D-5235. Technical discussions with P.N. Comley and D.G. Sanders (Boeing Company, Seattle, WA), who supplied the material, and Prof. C.S. Lee (Pohang University of Science and Technology, Pohang, Korea) are also greatly appreciated.

References

1. Y.T. Zhu, T.G. Langdon, R.Z. Valiev, S.L. Semiatin, D.H. Shin, and T.C. Lowe: *Ultrafine Grained Materials III*, TMS, Warrendale, PA, 2004

2. Y.T. Zhu, T.G. Langdon, Z. Horita, M.J. Zehetbauer, S.L. Semiatin, and T.C. Lowe, eds.: *Ultrafine Grained Materials IV*, TMS, Warrendale, PA, 2006.
3. M.J. Zehetbauer and R.Z. Valiev, eds.: *Proc. Second International Conference on Nanomaterials by Severe Plastic Deformation: Fundamentals-Processing-Applications*, Wiley-VCH, Weinheim, Germany, 2004.
4. A.K. Ghosh and C.H. Hamilton, *Metall. Trans. A*, 1979, vol. 10A, pp. 699-706.
5. S.M.L. Sastry, R.J. Lederich, T.L. Mackay, and W.R. Kerr, *J. Metals*, January 1983, vol. 35, no. 1, pp. 48-53.
6. H. Inagaki: *Z. fur Metallkunde*, 1995, vol. 86, pp. 643-650.
7. S.V. Zherebstov, G.A. Salishchev, R.M. Galeyev, O.R. Valiakhmetov, and S.L. Semiatin: *Proc. Second International Conference on Nanomaterials by Severe Plastic Deformation: Fundamentals-Processing-Applications*, M.J. Zehetbauer and R.Z. Valiev, eds., Wiley-VCH, Weinheim, Germany, 2004, pp. 835-840.
8. G.A. Salishchev, R.M. Galeyev, O.R. Valiakhmetov, R.V. Safiullin, R.Y. Lutfullin, O.N. Senkov, F.H. Froes, and O.A. Kaibyshcv: *J. Mater. Proc. Techn.*, 2001, vol. 116, pp. 265-68.
9. Y.G. Ko, C.S. Lee, D.H. Shin, and S.L. Semiatin: *Metall. and Mater. Trans. A*, 2006, vol. 37A, pp. 381-391.
10. A.K. Ghosh: Unpublished research, University of Michigan, Ann Arbor, MI, 2006.
11. A.V. Sergueeva, V.V. Stolyarov, R.Z. Valiev and A.K. Mukherjee: *Mater. Sci. Eng. A,* 2002, vol. A323, pp. 318-25.
12. R.S. Mishra, V.V. Stolyarov, C. Echer, R.Z. Valiev, and A.K. Mukherjee: *Mater. Sci. Eng. A,* 2001, vol. A298, pp. 44-50.

13. P.N. Comley: *J. Mater. Eng. Perf.*, 2004, vol. 13, pp. 660-664.
14. S.N. Patankar, J.P. Escobedo, D.P. Field, G. Salishchev, R.M. Galeyev, O.R. Valiakhmetov, and F.H. Froes: *J. Alloys and Compounds*, 2002, vol. 345, pp. 221-227.
15. P.N. Comley: *Mater. Sci. Forum*, 2004, vol. 447-448, pp. 233-238.
16. G.A. Sargent, A.P. Zane, P.N. Fagin, A.K. Ghosh, and S.L. Semiatin: *Metall. and Mater. Trans. A*, 2008, vol. 39A, pp. 2949-2964.
17. J.A. Wert and N.E. Paton: *Metall. Trans. A*, 1983, vol. 14A, pp. 2535-2544.
18. P.A. Friedman and A.K. Ghosh: *Metall. and Mater. Trans. A*, 1996, vol. 27A, pp. 3030-3042.
19. S.L. Semiatin and J.J. Jonas: *Formability and Workability of Metals: Plastic Instability and Flow Localization*, American Society for Metals, Metals Park, OH, 1984.
20. S.L. Semiatin, A.K. Ghosh, and J.J. Jonas: *Metall. Trans. A*, 1985, vol. 16A, pp. 2291-2298.
21. R.C. Gifkins: *Metall. Trans. A*, 1976, vol. 7A, pp. 1225-1232.
22. S.L. Semiatin, M.W. Corbett, P.N. Fagin, G.A. Salishchev, and C.S. Lee: *Metall. and Mater. Trans. A*, 2006, vol. 37A, pp. 1125-1136.
23. J.E. Bird, A.K. Mukherjee, and J. E. Dorn in: *Quantitative Relation Between Microstructure and Properties*, D.G. Brandon and A. Rosen, eds., Israel Universities Press, Jerusalem, Israel, 1969, pp. 255-342.
24. E.B. Shell and S.L. Semiatin: *Metall. and Mater. Trans. A*, 1999, vol. 30A, pp. 3219-3229.

25. S.L. Semiatin, V. Seetharaman, and I. Weiss: *Mater. Sci. Eng. A,* 1999, vol. A263, pp. 257-271.

26. S.L. Semiatin, N. Stefansson, and R.D. Doherty: *Metall. and Mater. Trans. A*, 2005, vol. 36A, pp. 1372-1376.

27. S.L. Semiatin and T.R. Bieler: *Acta Mater.*, 2001, vol. 49, pp. 3565-3573.

28. M.G. Zelin and A.K. Mukherjee: *Mater. Sci. Eng. A,* 1996, vol. A208, pp. 210-225.

Table I. Composition (Weight Pct.) of Ti-6Al-4V Sheet Materials*

Sheet ID	Al	V	Fe	O	C	H	N
A	6.23	4.22	0.29	0.14	<0.01	0.007	<0.005
B	6.08	4.37	0.26	0.14	0.005	0.005	<0.01

* Both alloys also contained small amounts (~0.1 weight percent) of Cr and Ni

Table II. Measured Dynamic (K_d) and Static (K_s) Coarsening Rate Constants for Sheet A

Temp (°C)	Strain Rate (s^{-1})	K_d ($\mu m^3/h$)	K_s ($\mu m^3/h$)	K_d/K_s
775	10^{-4}	3.9	0.56	7.0
775	10^{-3}	8.8	0.56	15.7
815	10^{-4}	6.8	0.87	7.8
815	10^{-3}	15.8	0.87	18.2

Figure Captions

Figure 1. BSEI micrographs of Ti-6Al-4V Sheet A: (a) As-received condition or (b) after a heat treatment at 775°C for 15 minutes followed by water quenching.

Figure 2. BSEI micrographs of Ti-6Al-4V Sheet B: (a) As-received condition or (b, c) after a heat treatment at 775°C for 15 minutes followed by water quenching.

Figure 3. Alpha-phase (0002) pole figures for the Ti-6Al-4V program materials in the as-received condition: (a) Sheet A and (b) Sheet B.

Figure 4. Sheet tension sample geometry.

Figure 5. True stress - true strain curves from constant strain rate tension tests for (a) Sheet A and (b) Sheet B.

Figure 6. Strain dependence of the m value determined from jump tests at the indicated strain rates for (a) Sheet A and (b) Sheet B.

Figure 7. Alpha-phase (0002) pole figures after deformation in uniaxial tension at 775°C and a strain rate of 10^{-3} s^{-1}: (a) Sheet A (local true strain ~2.1) and (b) Sheet B (local true strain ~2.4).

Figure 8. BSEI micrographs of Ti-6Al-4V Sheet A following tension testing at 775°C, 10^{-3} s^{-1}. The micrographs were taken at local true axial strains equal to: (a) 1.29, (b) 2.06, and (c) 2.46. The degree of dynamic coarsening is illustrated by comparison with the microstructure developed during heat treatment at 775°C for 15 minutes (followed by water quenching) shown in (d).

Figure 9. BSEI micrographs of Ti-6Al-4V Sheet A following tension testing at 775°C, 10^{-4} s^{-1}. The micrographs were taken at local true axial strains equal to: (a) 1.38, (b) 1.89, and (c) 2.03. The degree of dynamic coarsening is illustrated

by comparison with the microstructure developed during heat treatment at 775°C for 15 minutes (followed by water quenching) shown in (d).

Figure 10. BSEI micrographs of Ti-6Al-4V Sheet A following static-coarsening heat treatment at 775°C (followed by water quenching) for times of (a) 15 min, (b) 1 h, (c) 4 h, (d) 16 h, (e) 48 h, and (f) 96 h.

Figure 11. Static-coarsening measurements for Ti-6Al-4V Sheet A: (a) Cube of the average alpha-particle size as a function of time and (b) relationship between the alpha-particle size and the beta grain size. The results in (b) are compared to previous observations of the static coarsening behavior of an ultrafine Ti-6Al-4V billet material [16].

Figure 12. BSEI micrographs of Ti-6Al-4V Sheet B following tension testing at 775°C, 10^{-3} s^{-1}. The micrographs were taken at local true axial strains equal to: (a) 1.16, (b) 2.0, and (c) 2.42. The degree of dynamic coarsening is illustrated by comparison with the microstructure developed during heat treatment at 775°C for 15 minutes (followed by water quenching) shown in (d).

Figure 13. BSEI micrographs of Ti-6Al-4V Sheet B following tension testing at 775°C, 10^{-4} s^{-1}. The micrographs were taken at local true axial strains equal to: (a) 1.29, (b) 1.78, and (c) 2.15. The degree of dynamic coarsening is illustrated by comparison with the microstructure developed during heat treatment at 775°C for 15 minutes (followed by water quenching) shown in (d).

Figure 14. Flow-localization model predictions of stress-strain response for m = 0.5 and f_o = 0.98: (a) comparison of the engineering stress-strain curve and the true

stress – true strain curve based on uniform deformation assumption for a non-hardening material and (b) comparison of true stress – true strain curves for a non-hardening and a flow-hardening material.

Figure 15. Flow-localization model predictions of plastic flow behavior of a non-hardening material for various values of m and f_o: (a) True stress – true strain curves and (b) true strain profiles after sample extension to an average (overall) true strain of 1.9. In (b), the center of the neck is located at 0 mm, and the end of the gage section is at ~42.5 mm.

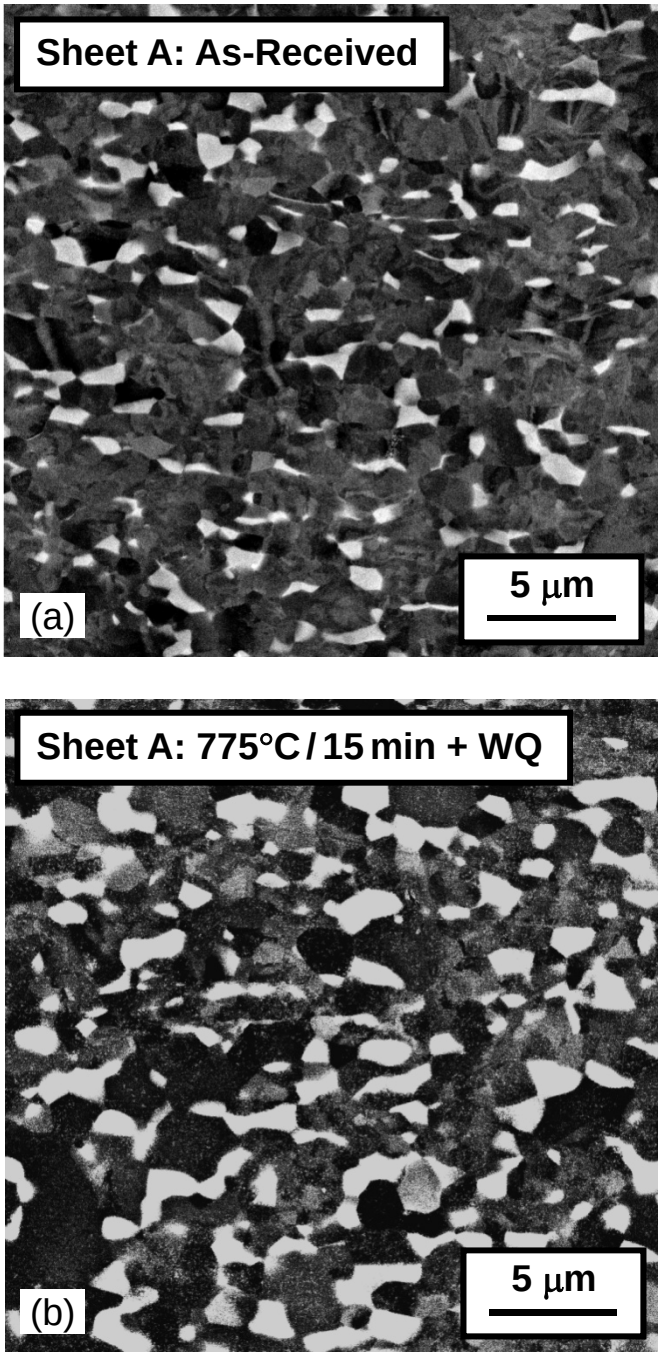

Figure 1. BSEI micrographs of Ti-6Al-4V Sheet A: (a) As-received condition or (b) after a heat treatment at 775°C for 15 minutes followed by water quenching.

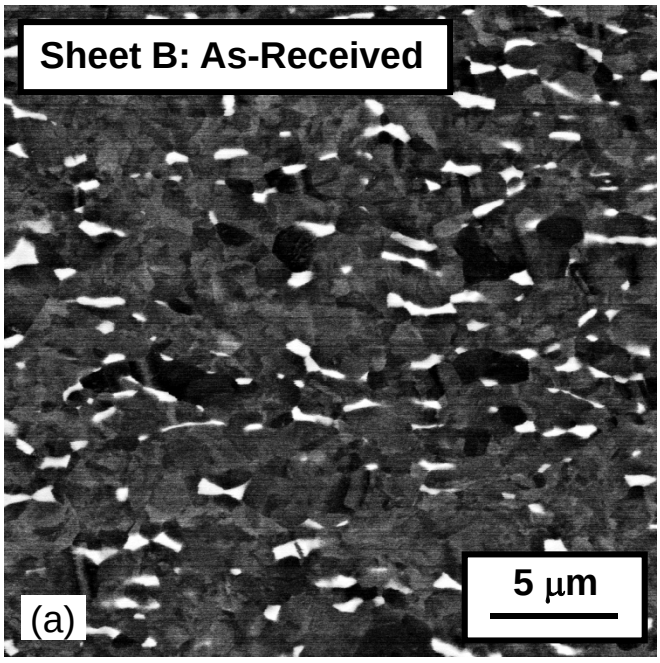

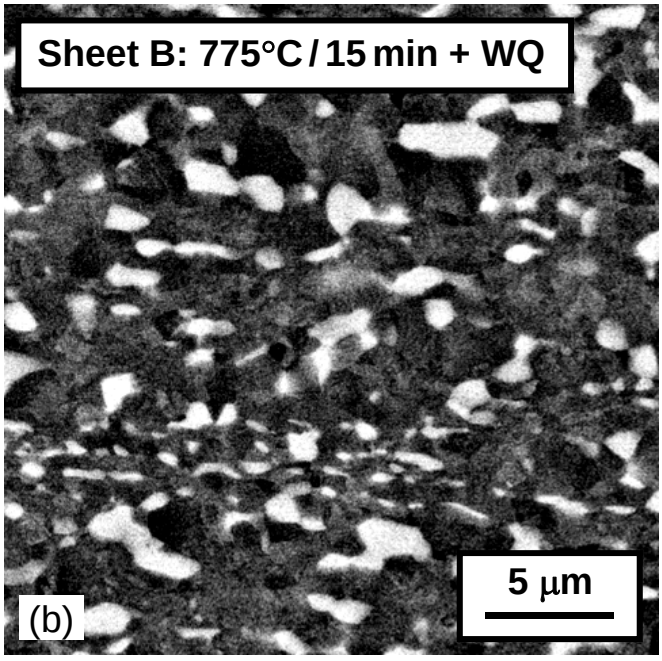

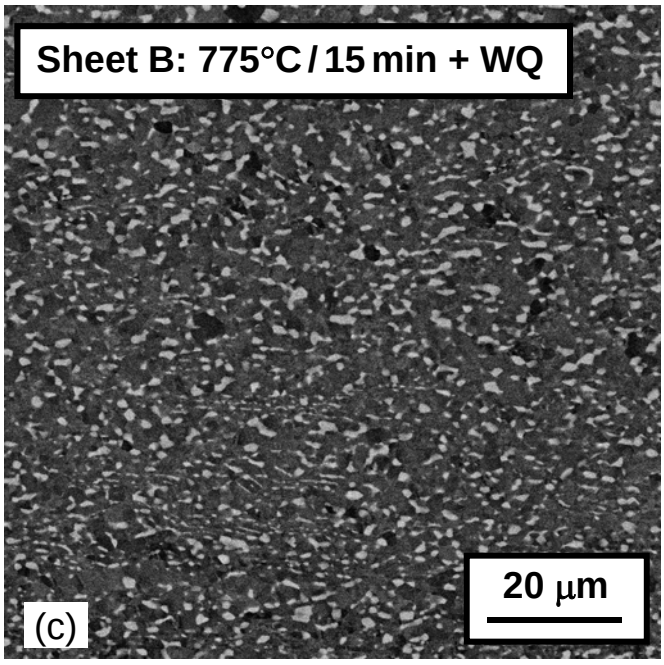

Figure 2. BSEI micrographs of Ti-6Al-4V Sheet B: (a) As-received condition or (b, c) after a heat treatment at 775°C for 15 minutes followed by water quenching.

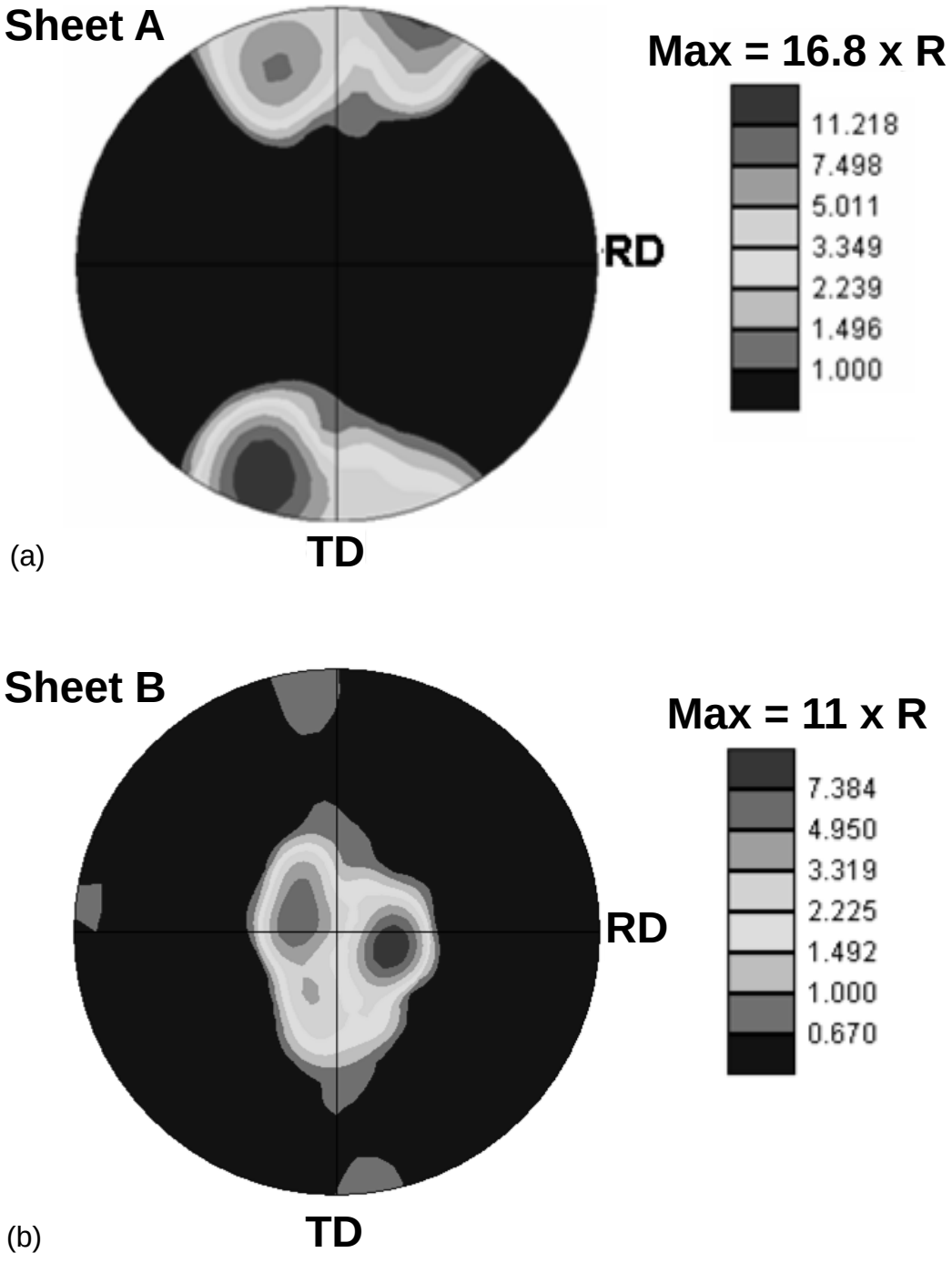

Figure 3. Alpha-phase (0002) pole figures for the Ti-6Al-4V program materials in the as-received condition: (a) Sheet A and (b) Sheet B.

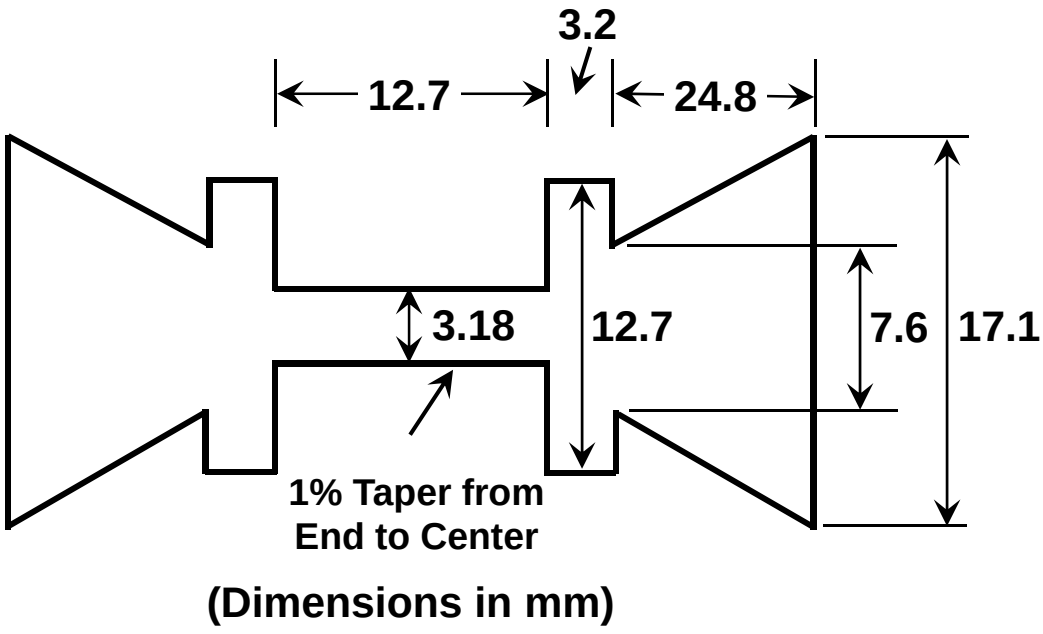

Figure 4. Sheet tension sample geometry.

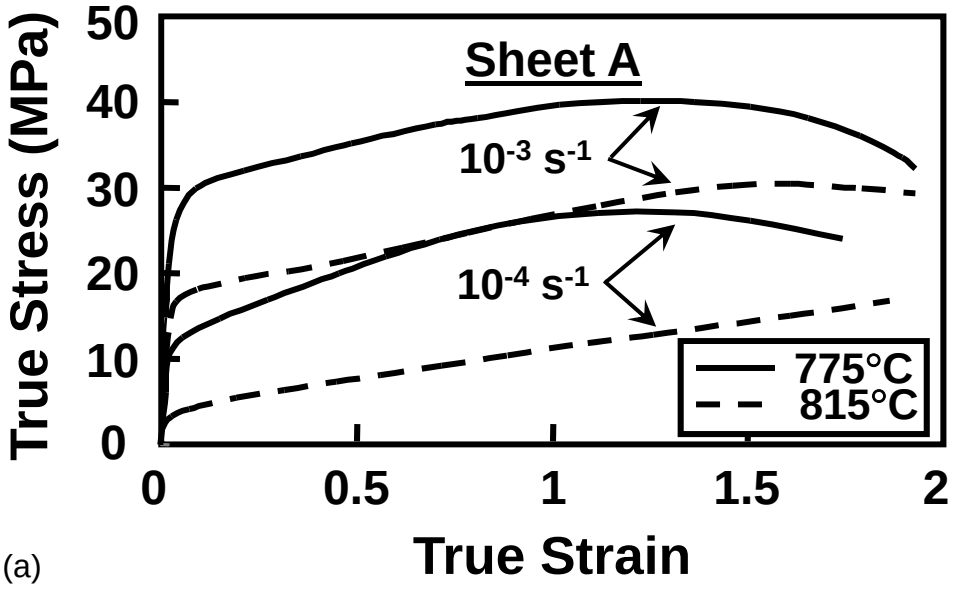

(a)

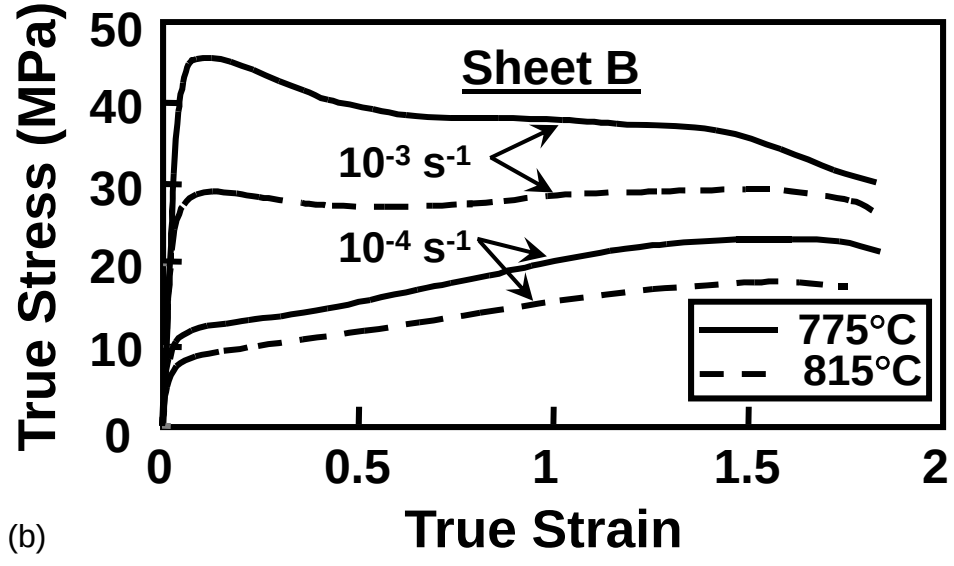

(b)

Figure 5. True stress - true strain curves from constant strain rate tension tests for (a) Sheet A and (b) Sheet B.

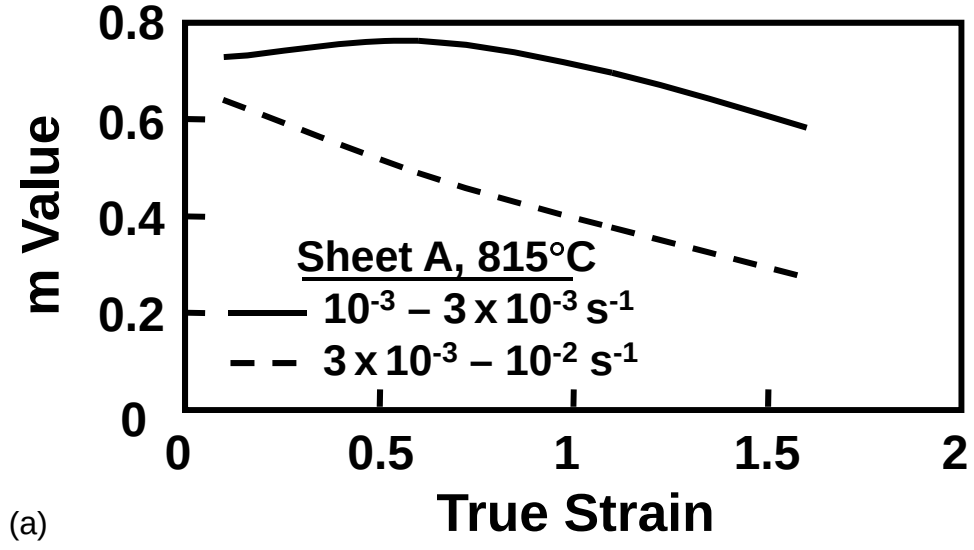

(a)

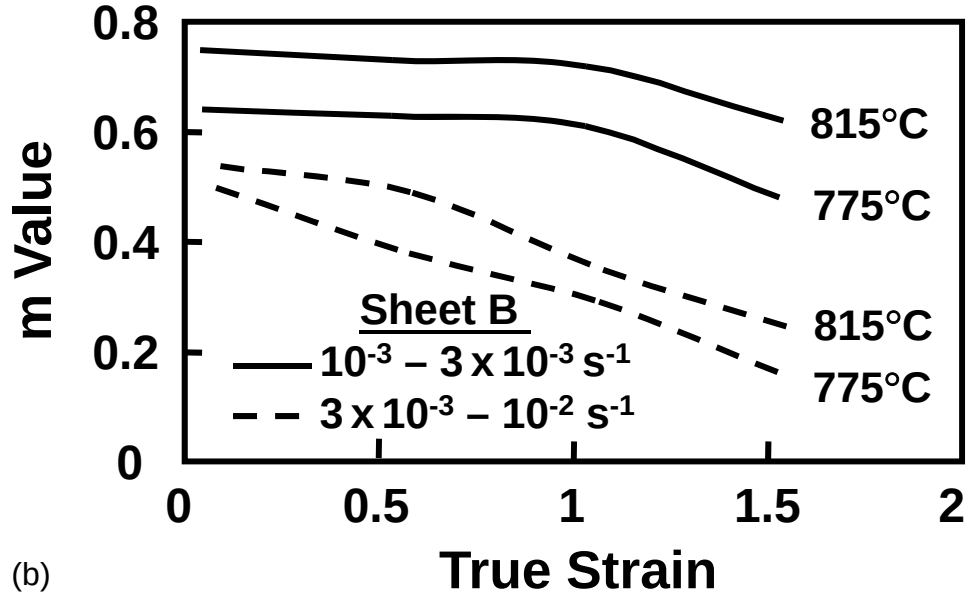

(b)

Figure 6. Strain dependence of the m value determined from jump tests at the indicated strain rates for (a) Sheet A and (b) Sheet B.

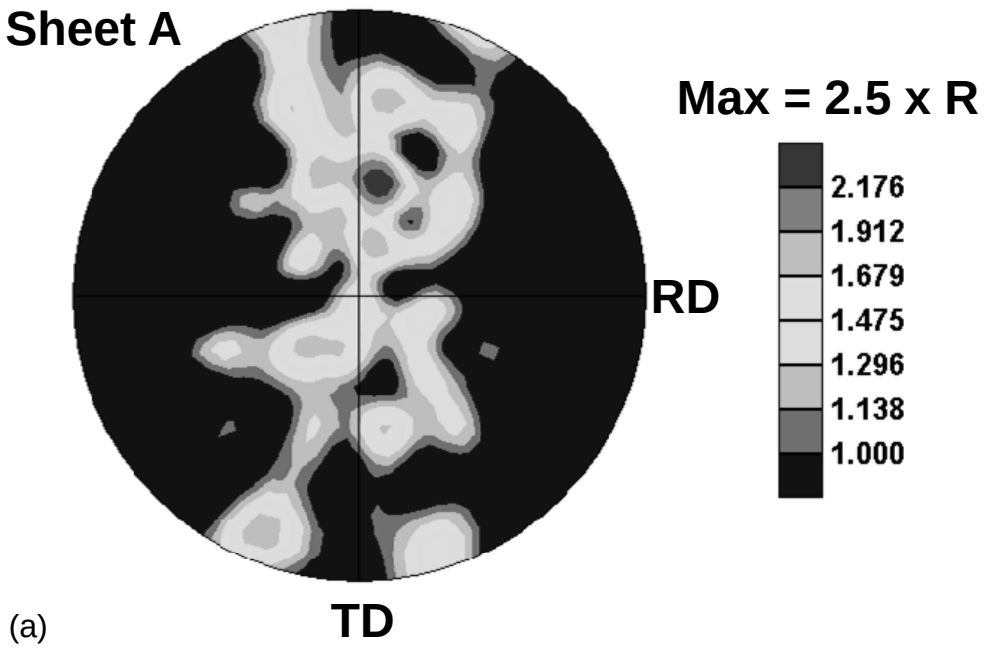

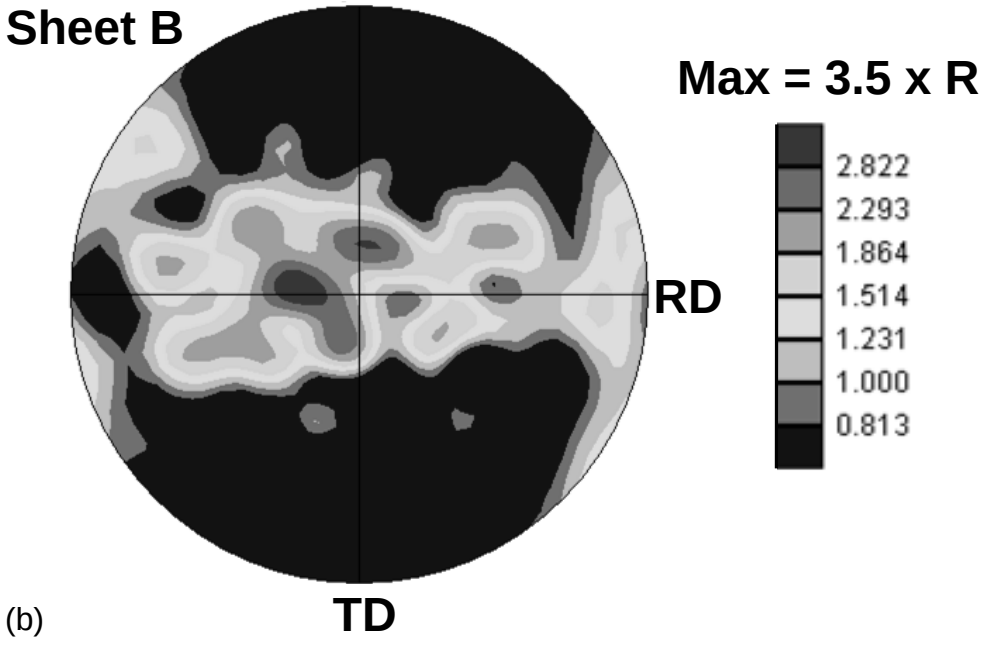

Figure 7. Alpha-phase (0002) pole figures after deformation in uniaxial tension at 775°C and a strain rate of 10^{-3} s^{-1}: (a) Sheet A (local true strain ~2.1) and (b) Sheet B (local true strain ~2.4).

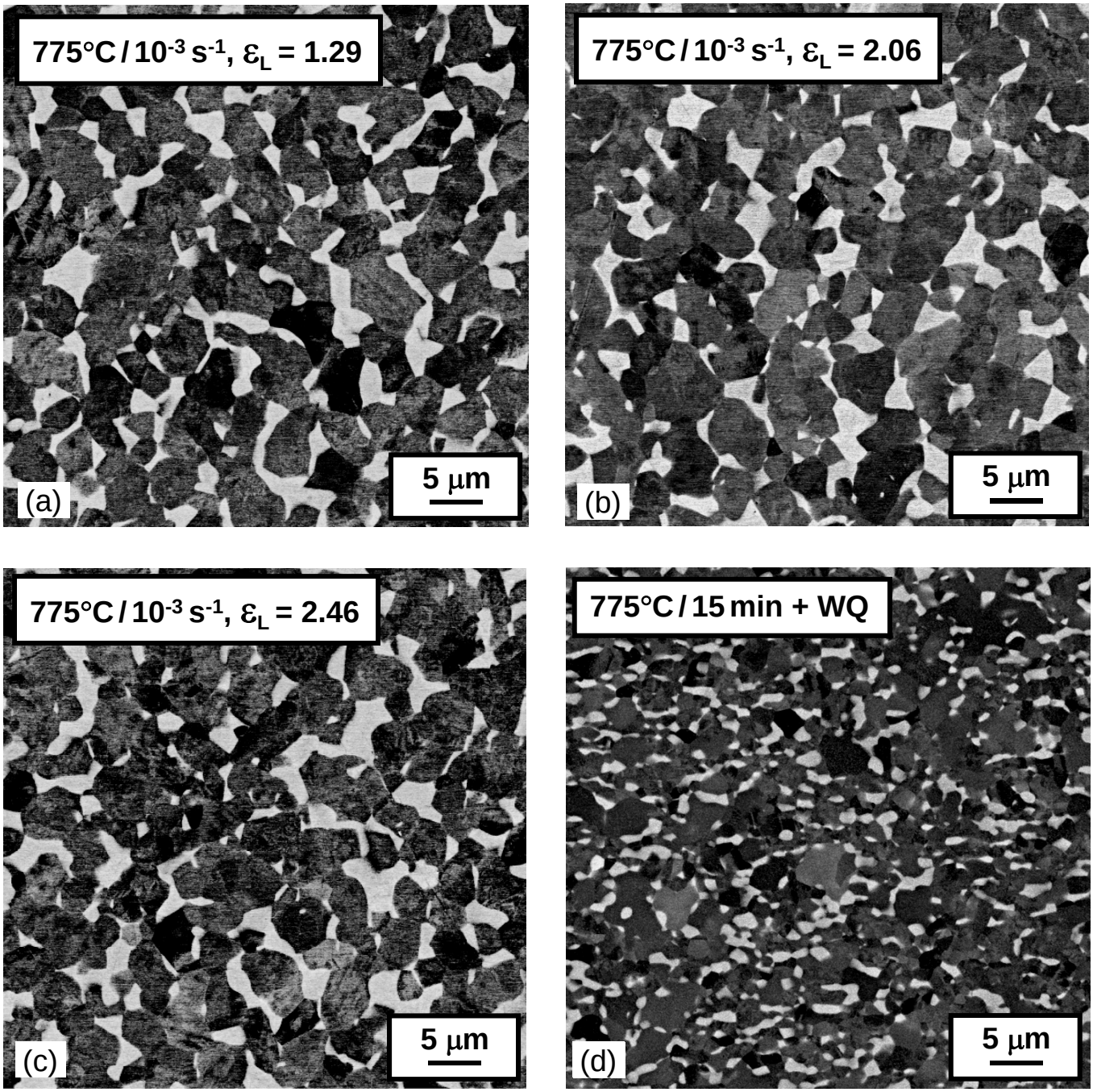

Figure 8. BSEI micrographs of Ti-6Al-4V Sheet A following tension testing at 775°C, 10^{-3} s^{-1}. The micrographs were taken at local true axial strains equal to: (a) 1.29, (b) 2.06, and (c) 2.46. The degree of dynamic coarsening is illustrated by comparison with the microstructure developed during heat treatment at 775°C for 15 minutes (followed by water quenching) shown in (d).

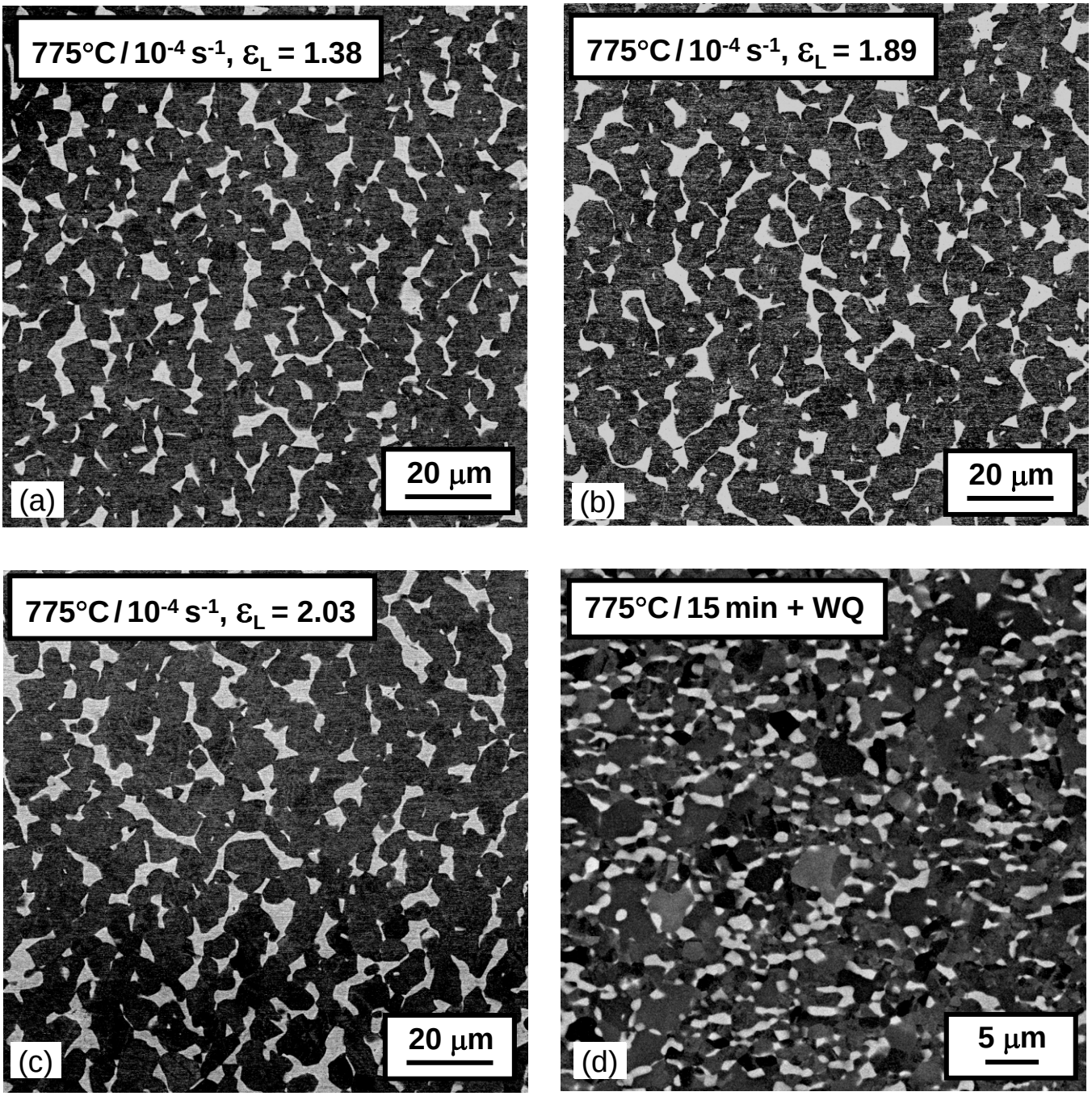

Figure 9. BSEI micrographs of Ti-6Al-4V Sheet A following tension testing at 775°C, 10^{-4} s^{-1}. The micrographs were taken at local true axial strains equal to: (a) 1.38, (b) 1.89, and (c) 2.03. The degree of dynamic coarsening is illustrated by comparison with the microstructure developed during heat treatment at 775°C for 15 minutes (followed by water quenching) shown in (d).

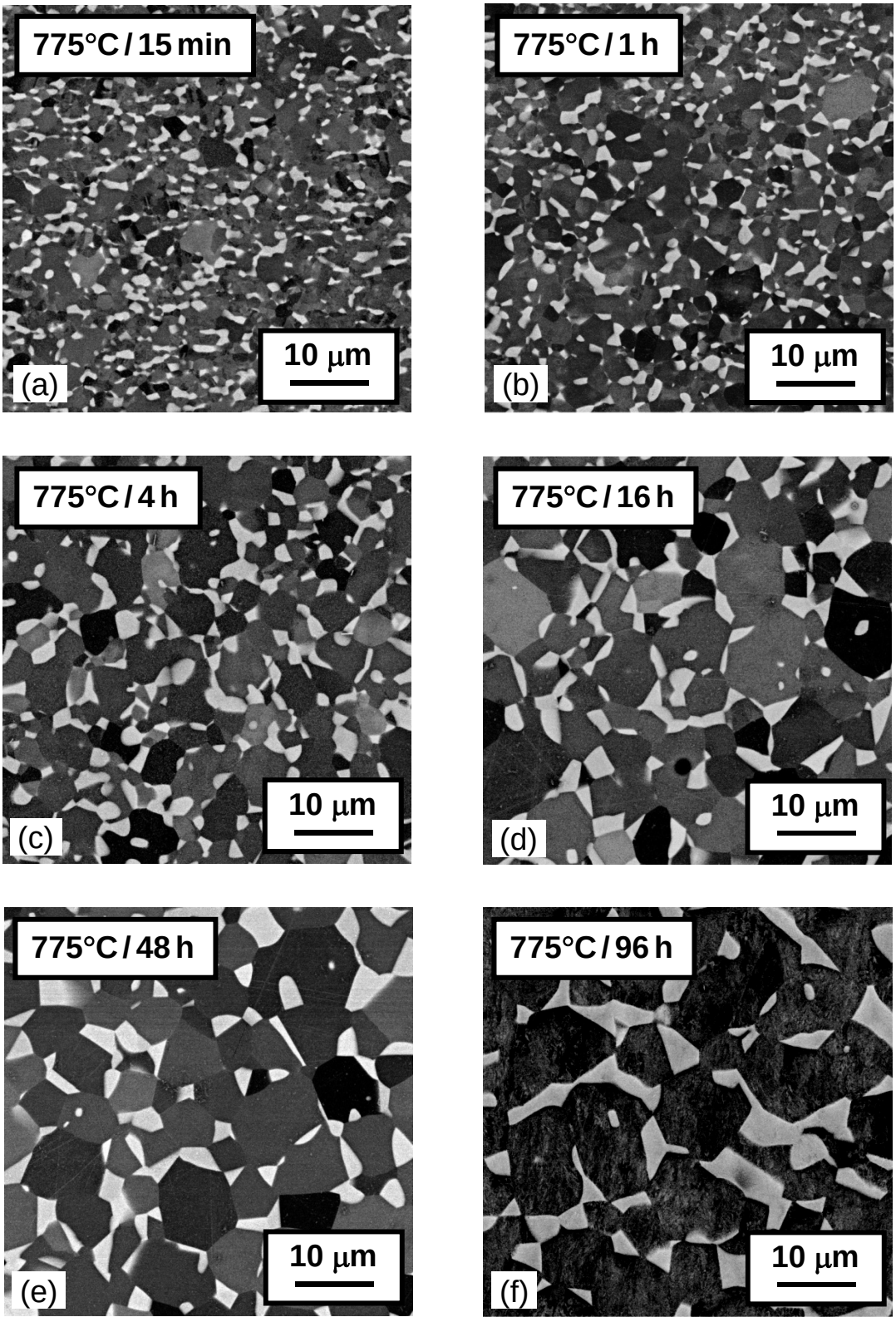

Figure 10. BSEI micrographs of Ti-6Al-4V Sheet A following static-coarsening heat treatment at 775°C (followed by water quenching) for times of (a) 15 min, (b) 1 h, (c) 4 h, (d) 16 h, (e) 48 h, and (f) 96 h.

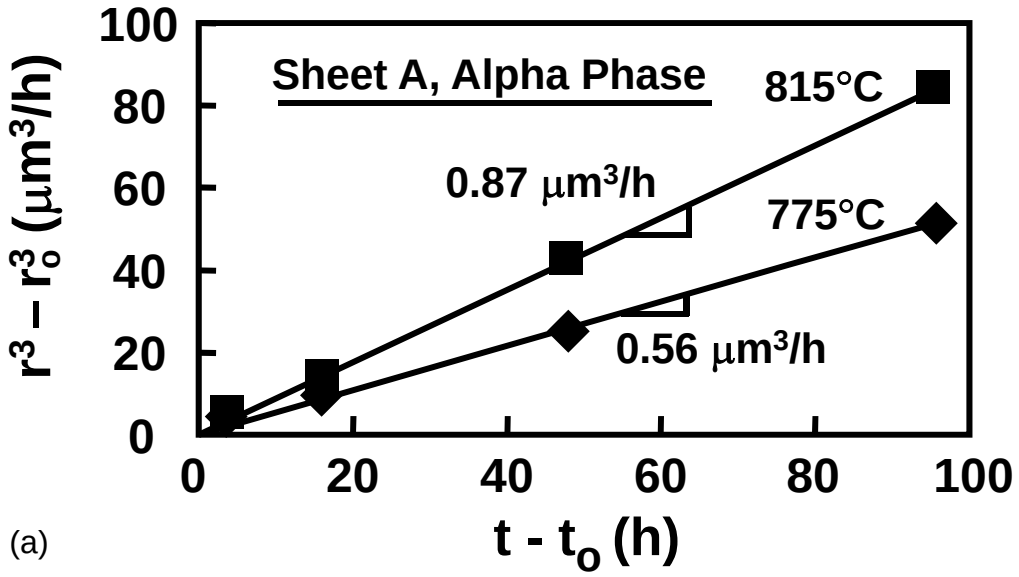

(a)

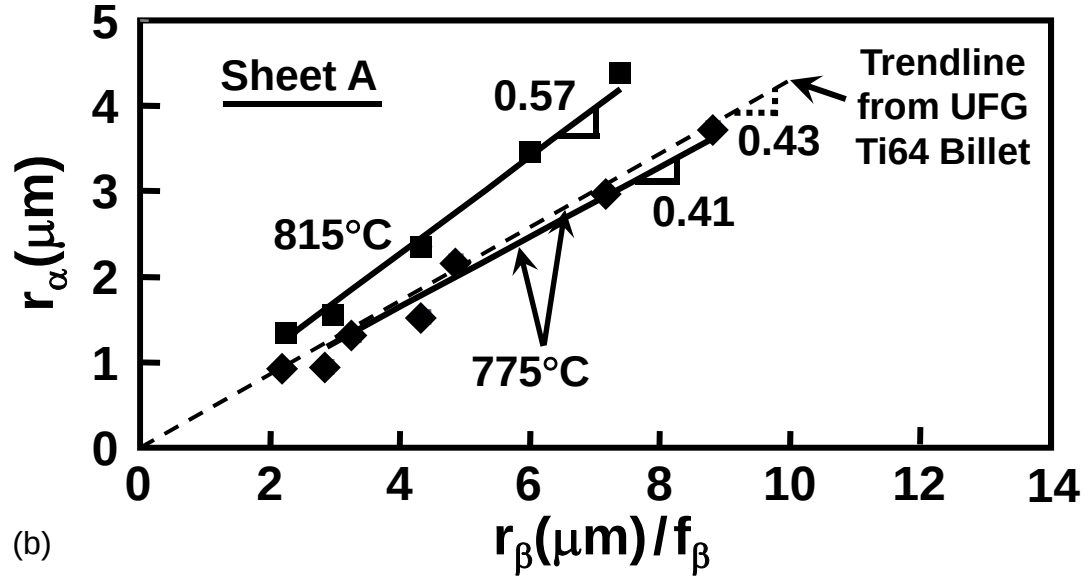

(b)

Figure 11. Static-coarsening measurements for Ti-6Al-4V Sheet A: (a) Cube of the average alpha-particle size as a function of time and (b) relationship between the alpha-particle size and the beta grain size. The results in (b) are compared to previous observations of the static coarsening behavior of an ultrafine Ti-6Al-4V billet material [16].

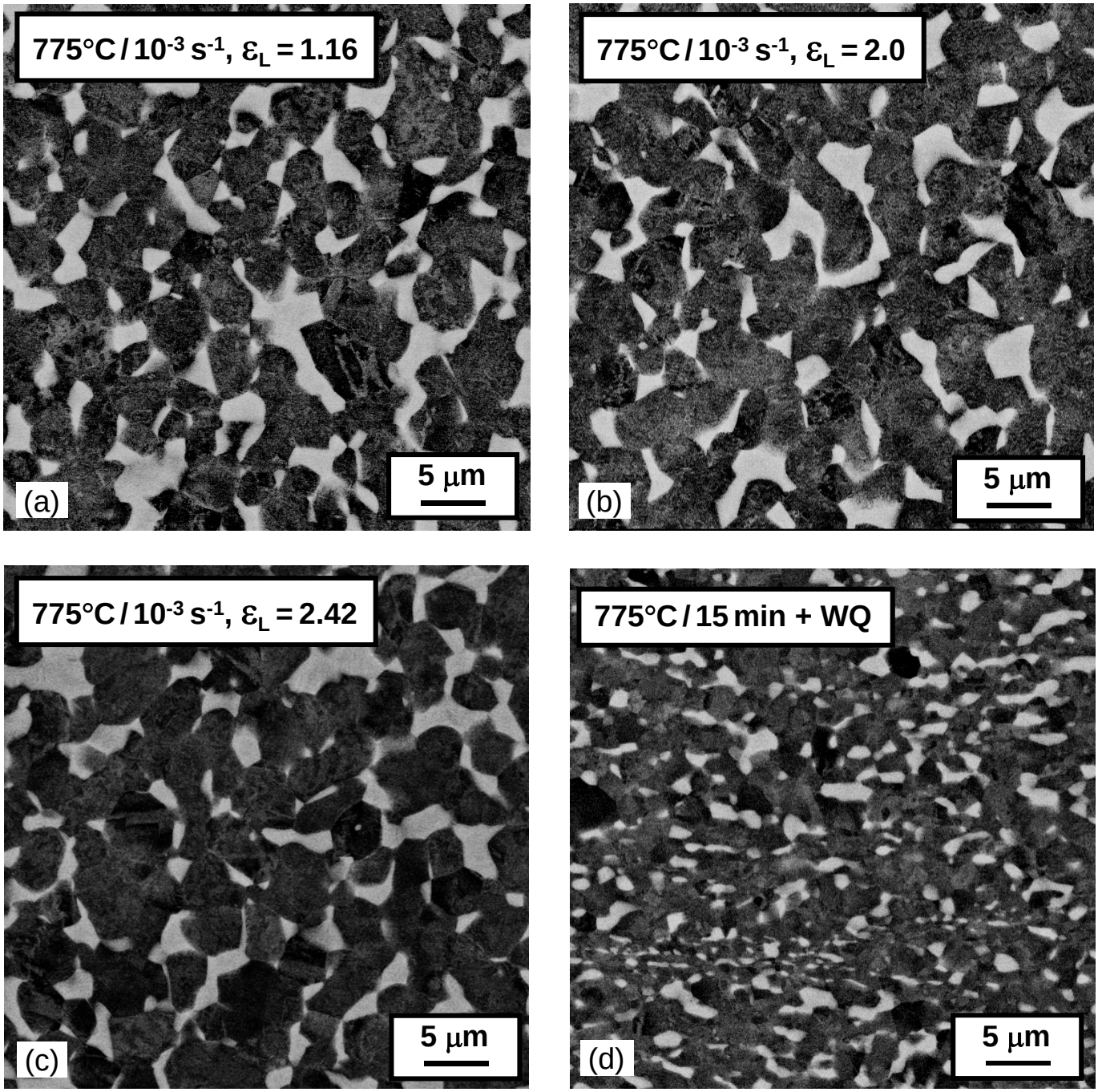

Figure 12. BSEI micrographs of Ti-6Al-4V Sheet B following tension testing at 775°C, 10^{-3} s^{-1}. The micrographs were taken at local true axial strains equal to: (a) 1.16, (b) 2.0, and (c) 2.42. The degree of dynamic coarsening is illustrated by comparison with the microstructure developed during heat treatment at 775°C for 15 minutes (followed by water quenching) shown in (d).

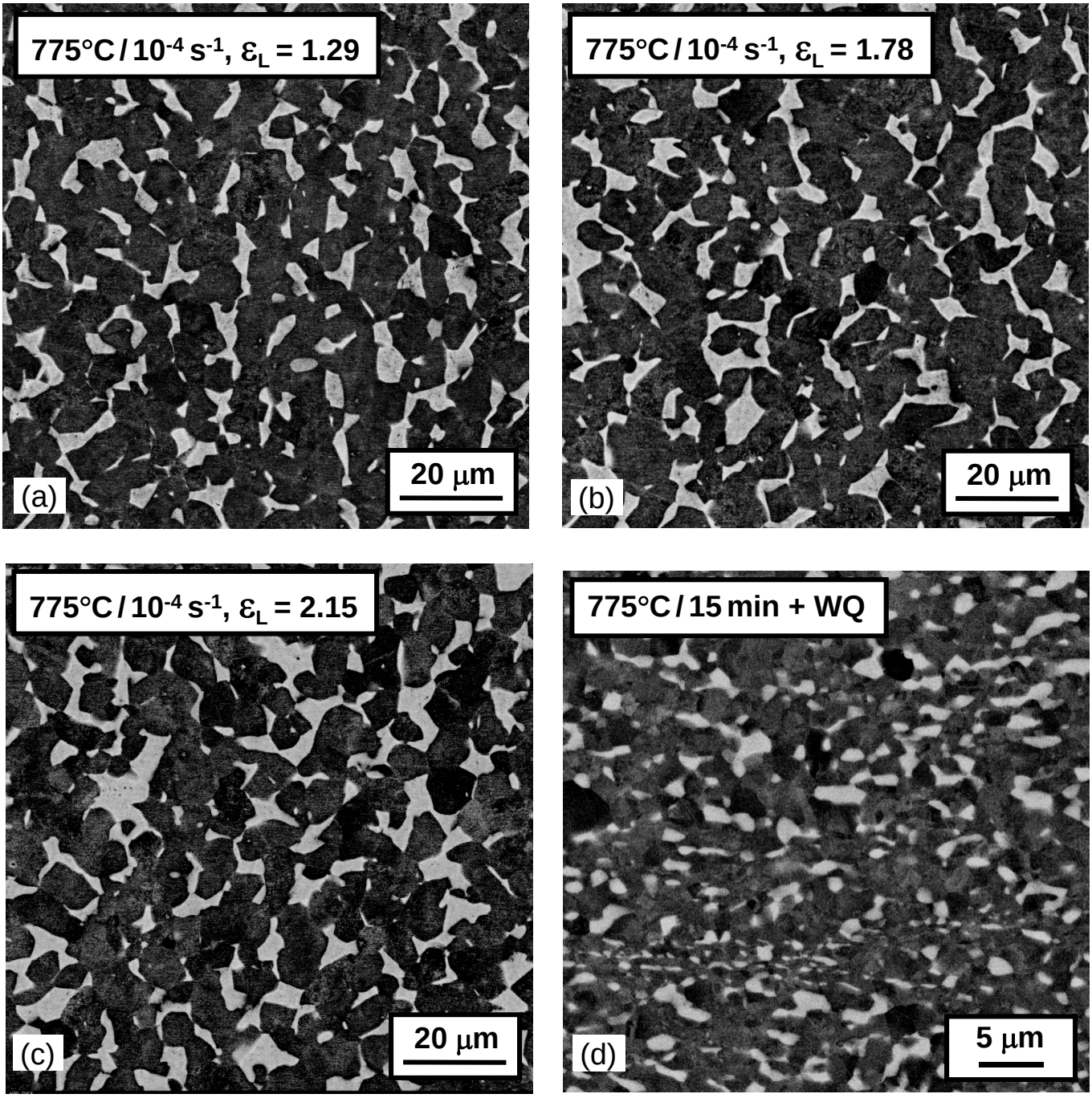

Figure 13. BSEI micrographs of Ti-6Al-4V Sheet B following tension testing at 775°C, 10^{-4} s^{-1}. The micrographs were taken at local true axial strains equal to: (a) 1.29, (b) 1.78, and (c) 2.15. The degree of dynamic coarsening is illustrated by comparison with the microstructure developed during heat treatment at 775°C for 15 minutes (followed by water quenching) shown in (d).

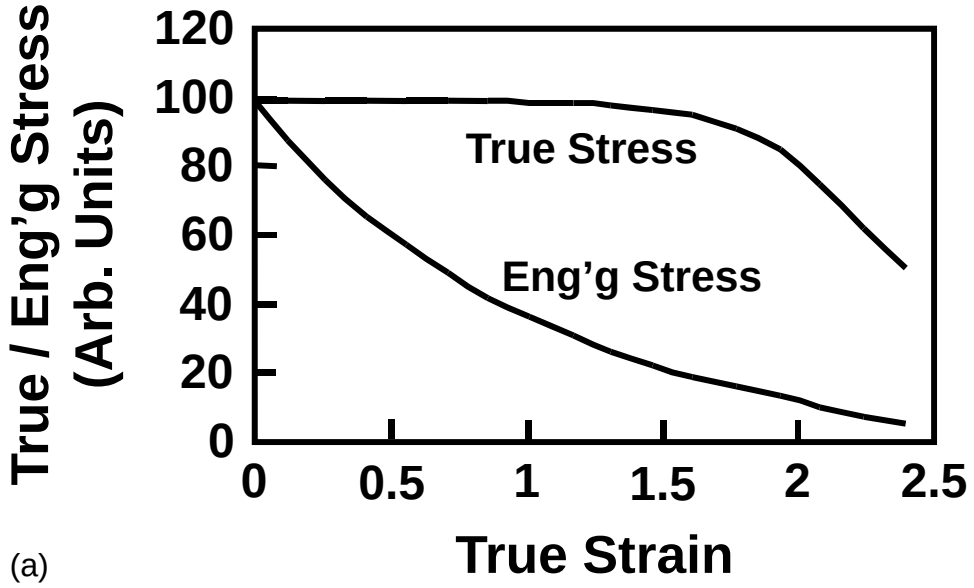

(a)

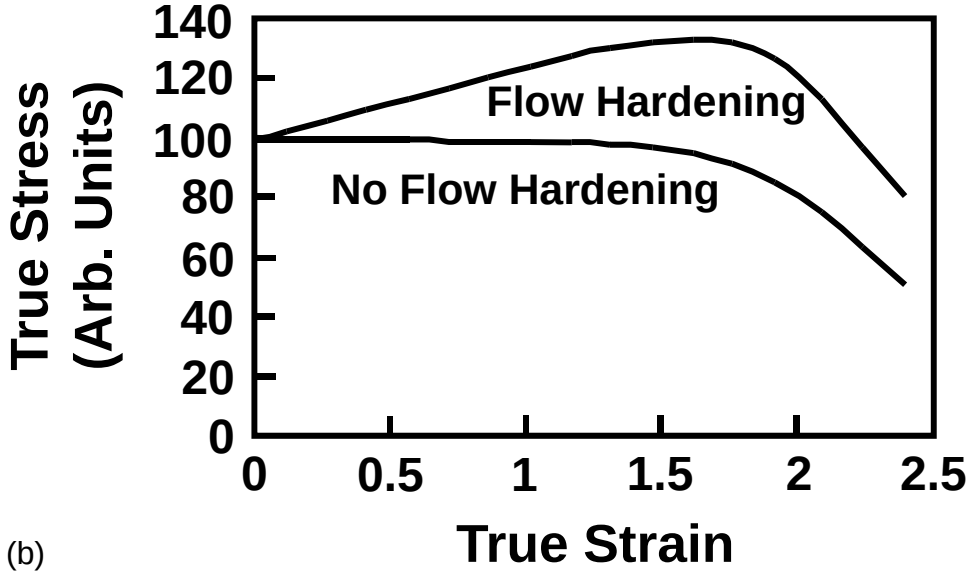

(b)

Figure 14. Flow-localization model predictions of stress-strain response for m = 0.5 and f_o = 0.98: (a) comparison of the engineering stress-strain curve and the true stress – true strain curve based on uniform deformation assumption for a non-hardening material and (b) comparison of true stress – true strain curves for a non-hardening and a flow-hardening material.

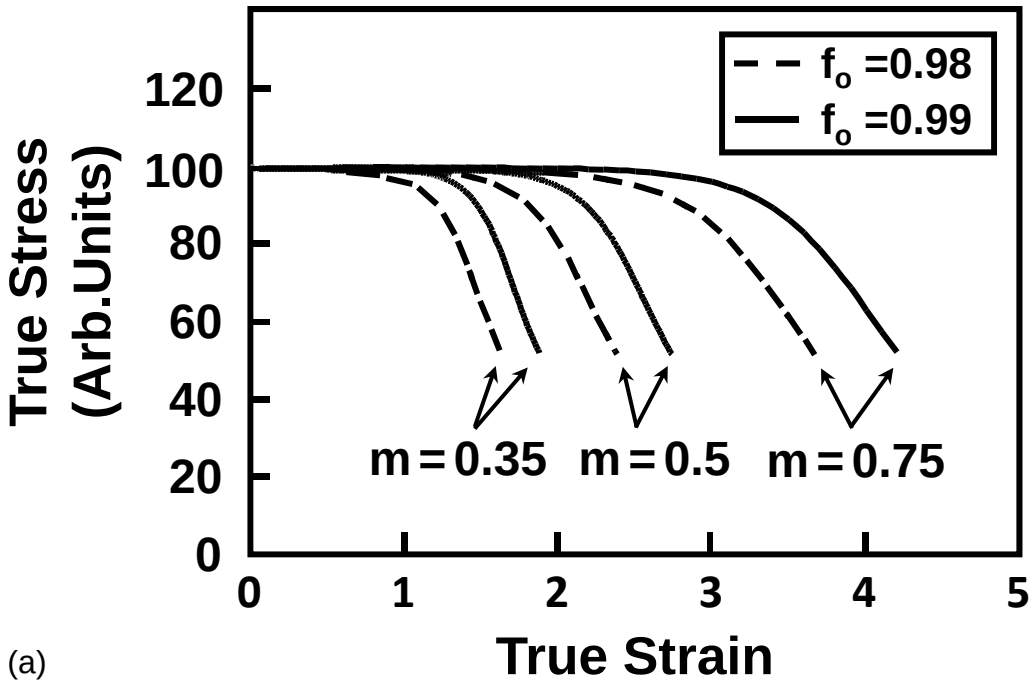

(a)

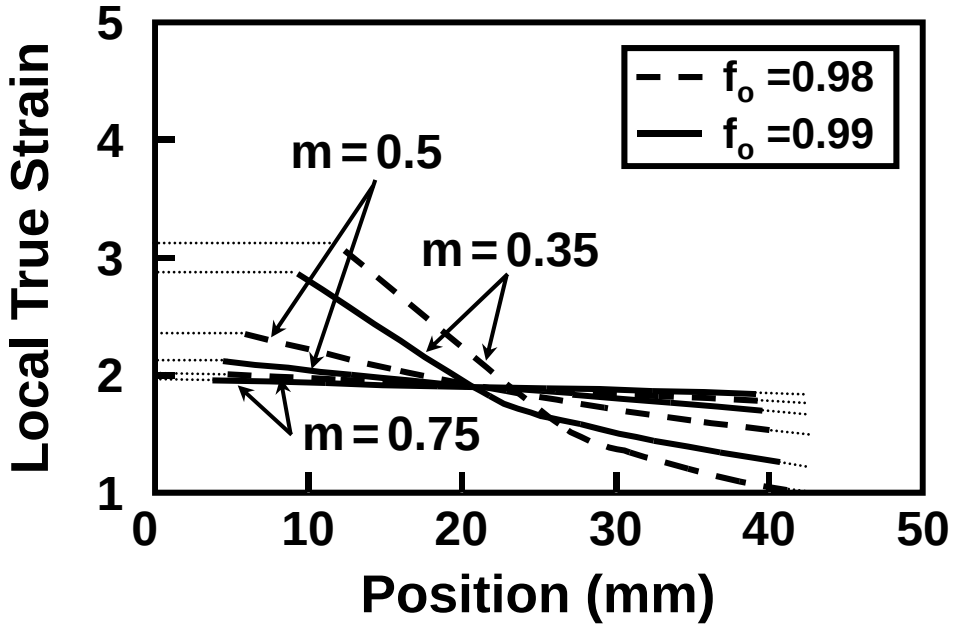

(b)

Figure 15. Flow-localization model predictions of plastic flow behavior of a non-hardening material for various values of m and f_o: (a) True stress – true strain curves and (b) true strain profiles after sample extension to an average (overall) true strain of 1.9. In (b), the center of the neck is located at 0 mm, and the end of the gage section is at ~42.5 mm.

Extra Figures